Title

Inter-eruptive volcanism at Usu volcano: Micro-earthquakes and dome subsidence

Authors

Hiroshi Aoyama (Corresponding Author)

Institute of Seismology and Volcanology, Graduate School of Science, Hokkaido University

N10W8, Kita-ku, Sapporo, Hokkaido

060-0810, Japan.

Tel: +81-11-706-4845, Fax: +81-11-746-7404

E-mail: aoyama@uvo.sci.hokudai.ac.jp

Shin'ya Onizawa

Geological Survey of Japan, AIST

Central 7 Higashi 1-1-1, Tsukuba, Ibaraki

305-8567, Japan.

E-mail: s-onizawa@aist.go.jp

Tomokadu Kobayashi

Institute of Seismology and Volcanology, Graduate School of Science, Hokkaido University

N10W8, Kita-ku, Sapporo, Hokkaido

060-0810, Japan

E-mail: tkoba@uvo.sci.hokudai.ac.jp

Takeshi Tameguri

Sakurajima Volcano Research Center, Disaster Prevention Research Institute, Kyoto University

1722-19, Sakurajima Yokoyama-cho, Kagoshima, Kagoshima

891-1419, Japan

E-mail: tamekuri@svo.dpri.kyoto-u.ac.jp

Takeshi Hashimoto

Institute of Seismology and Volcanology, Graduate School of Science, Hokkaido University

N10W8, Kita-ku, Sapporo, Hokkaido

060-0810, Japan

E-mail: hasimoto@uvo.sci.hokudai.ac.jp

Hiromitsu Oshima
Usu Volcano Observatory, Institute of Seismology and Volcanology, Graduate School of Science, Hokkaido University
Tatsuka 142, Sobetsu, Hokkaido
052-0106, Japan
E-mail: oshima@uvo.sci.hokudai.ac.jp

Hitoshi Y. Mori
Institute of Seismology and Volcanology, Graduate School of Science, Hokkaido University
N10W8, Kita-ku, Sapporo, Hokkaido
060-0810, Japan
E-mail: mori@uvo.sci.hokudai.ac.jp

Abstract.

Post-eruptive crustal activity after the 2000 eruption of Usu volcano was investigated by seismic and geodetic field observations. Remarkable features of the magmatic eruptions that occur almost every 30 years include lava dome formation and strong precursory earthquakes. On the other hand, rapid dome subsidence was observed by electronic distance meter (EDM) measurement after the 1977–1982 summit eruption. Since the 2000 eruption, seismic activity at a shallow part under the summit crater has remained at a high level relative to that after the 1977–1982 eruption, although eruption occurred at the western foot of the volcano during the 2000 eruption. To reveal the shallow crustal activity in the inter-eruptive period around the summit area, seismicity and crustal deformation have been investigated since 2006. Dense temporary seismic observations and hypocenter relocation analysis using a three-dimensional velocity structure model revealed that the focal area is localized along the U-shaped fault that developed in the dome-forming stage of the 1977–1982 eruption. Three major focal clusters are distributed on the southwestern side of Usu-Shinzan cryptodome, which was built up during the 1977–1982 eruption. For the seven major events with magnitudes larger than 1, the focal mechanism was a large dip-slip component, which suggests the subsidence of Usu-Shinzan cryptodome. Interferomatetric satellite aperture radar (InSAR) image analysis and repeated GPS measurements revealed subsidence of the summit dome, which is almost centered at the Usu-Shinzan cryptodome. The area of rapid deformation is restricted to a small area around the summit crater. The estimated rate of dome subsidence relative to the crater floor is about 3 cm/year. These results strongly suggest that subsidence of Usu-Shinzan is associated with the small earthquakes along the U-shaped fault that surrounds the cryptodome. According to prior seismic and geodetic studies, it is thought that most of the magma rising under the summit crater during the 2000 eruption stopped around a depth of 2 km below sea level, which is sufficiently deep relative to the focal area of the present seismicity. A part of magma intruded under the western foot and contributed to the 2000 eruption. We conclude that the 2000 eruption scarcely affected the shallow crustal activity under the summit crater, and that Usu-Shinzan cryptodome is continuing to subside just as it was before the 2000 eruption. The shallow volcanic earthquakes that began increasing from 1995 are closely related to the successive subsidence of the summit domes. Temporal change in fumarole temperature suggests a relationship between the shallow earthquakes and cooling of the magma that intruded under Usu-Shinzan during the 1977–1982 eruption.

Keywords:

Usu volcano, inter-eruptive activity, volcanic earthquakes, dome subsidence, InSAR analysis

1. Introduction

Volcanic eruptions larger than a certain magnitude usually repeat at long time intervals at the same volcano (e.g., Simkin and Siebert, 2000). An understanding of both eruptive and inter-eruptive activity is needed to get a true picture of volcanic processes. Eruptive as well as inter-eruptive volcanism has been investigated at many active volcanoes around the world. For example, more than 30 volcanoes are continuously monitored with observational instruments in Japan. Most of these volcanoes are now in a dormant period. Despite this long-term monitoring, our knowledge of inter-eruptive activities is still poor even for well-studied volcanoes. One reason is the long recurrence period of magmatic eruptions at a volcano. Except for currently active volcanoes, such as Kilauea in Hawaii, Stromboli in Italy, and Sakurajima in Japan, the recurrence periods of eruptions are longer than a few decades. Although volcano monitoring networks have recently become common at active volcanoes, we have only 30–40 years of data, even in the cases of well-studied volcanoes. If a volcano has a longer recurrence period for eruptions, and if our monitoring has been restricted to the dormant period, it is very hard to obtain information about magmatic activities from the monitoring data. The second reason is the quietness of crustal activities at a volcano during the dormant period. Volcanic earthquakes, fumarolic activities, and other phenomena can be observed even in the dormant period. However, it is generally hard to evaluate whether the observed phenomena provide worthwhile information about magmatic activity. Therefore, observational research on magmatic activities has largely focused on the active period.

The magmatic activity associated with an eruption declines, and preparation toward the next eruption quietly progresses under the volcano during the inter-eruptive period. Dzurisin et al. (2002) compared the results of leveling surveys at Medicine Lake volcano in 1954 and 1988–1990. They found remarkable subsidence near the caldera and attributed it to gravitational loading of thermally weakened crust by the mass of the volcano and associated intrusive rocks. Using interferometric synthetic aperture radar (InSAR) images, Lu et al. (2002) revealed a subsidence area of approximately 3 km in diameter at the summit of Kiska volcano in the western Aleutians. An elastic Mogi-type deformation analysis suggested a shallow source, and they attributed the subsidence to decreased pore-fluid pressure within a shallow hydrothermal system beneath the summit area. Deformations of emplaced lava flows have also been reported at several volcanoes (Briole et al., 1997, Furuya, 2004, Lu et al., 2005, Stevens et al., 2001). These deformations were interpreted as the result of viscoelastic relaxation, compaction, and/or thermoelastic contraction. The above studies indicate that ground subsidence has been widely observed during the inter-eruptive period and suggest that the emplacement and cooling of magma play key roles in inter-eruptive volcanism.

Usu volcano offers a good opportunity for studying the inter-eruptive volcanism of a dacitic volcano. Magmatic eruptions have occurred at Usu four times during the 20th century, causing

considerable damage to the property of residents around the volcano. The last eruption was in 2000, and the next magmatic eruption is expected to occur within a few decades. Because preparations for the next eruption must eventually be made, it is important to understand the inter-eruptive activity in detail now. Modern physical monitoring recorded magmatic eruptions twice in the late 20th century. Many researchers have studied the volcanic phenomena associated with eruptions and short-term precursors, and new information has become available about the dacitic volcanism associated with lava dome formation (e.g., Okada et al., 1981, Yokoyama et al., 1981). In contrast to the vigorous volcanism in the eruptive period, volcanoes are believed to remain dormant during the inter-eruptive period, with the exception of long-term subsidence of lava domes (Mori and Suzuki, 1998). Similar to the study by Dzurisin et al. (2002), the dome subsidence of Usu volcano had been monitored in the traditional manner by repeated geodetic measurements. Therefore, data were not abundant in spatial and temporal coverage. After the 2000 eruption, improvements in monitoring techniques were made to better record the crustal activities in the summit crater in the dormant period, including shallow volcanic earthquakes and continued lava dome subsidence. To investigate the activities during the inter-eruptive period in detail, temporary dense seismic observation, GPS measurements, and InSAR analysis were carried out. Our research presented here will bridge the gap between understanding the eruptive and inter-eruptive volcanism of Usu volcano.

This paper reports the precise distribution of the hypocenters and the focal mechanisms of dominant earthquakes that occurred from early June until late August 2006. The spatial extent of the lava dome subsidence was estimated from InSAR analysis, and the subsiding rate was determined by GPS measurements. It seems that these two phenomena are closely related to the cryptodome growth during the summit eruption in 1977–1982. Section 2 briefly introduces the recent eruptions of Usu volcano. Previous studies on inter-eruptive activities and subsurface structures are then reviewed in section 3. Section 4 presents seismic observations from 2006 and related analyses. In section 5, the results of InSAR and GPS analyses are introduced. Finally, we discuss the relationships between the 1977–1982 eruption and present volcanism in section 6. In the conclusion, we propose a preliminary model for the crustal activity at Usu volcano, which includes results of past research.

2. Recent eruptions of Usu volcano

Usu volcano is situated on the southern rim of Toya caldera in western Hokkaido and has experienced magmatic eruptions almost every 30 years (Fig. 1). Its highest peak is about 700 m above sea level, and its base is approximately 6 km in diameter. Two lava domes, Ko-Usu and O-Usu are located within the summit crater, which has a diameter of about 2 km. The volcano is very famous for its characteristic volcanism, which includes lava dome and cryptodome growth and strong precursory seismicity. The volcano is now in an active phase from the perspective of the geological timescale; a sequence of eruptions in the current phase began in 1663, after a dormant phase of 7000 years. Since the 1663 eruption, nine eruptive activities have occurred. The Ko-Usu and O-Usu lava domes are considered to have been formed by the 1663 and 1853 eruptions, respectively (e.g., Yokoyama et al., 1973). Four eruptions occurred in the 20th century, in 1910, 1943–1945, 1977–1982, and 2000. All of these eruptions were observed by physical monitoring instruments.

The first seismological monitoring during an eruption of Usu volcano was executed by Dr. Omori during the 1910 eruption. Using his original seismometer, he found continuous ground vibration associated with the eruption (Omori, 1911). Following four days of precursory felt earthquakes, numerous craters opened at the northern slope. A part of the crater area was uplifted and made a new peak, called Meiji-Shinzan.

After 33 years of quiescence, precursory earthquakes began on December 28, 1943. One month later, a swell was observed at the southeastern foot of the volcano. From April 1944, the swell migrated northward and eruption began from the elevated area in late June. The ground uplift continued until September 1945, finally creating a new mountain with a height of 406.9 m. This mountain was named Showa-Shinzan and is located at the eastern foot of Usu volcano. A seismic monitoring network was deployed by Dr. Minakami during the eruption (Minakami et al., 1951). The locations of the hypocenters were determined using the seismograms from five temporary stations. Precursory deep earthquakes having clear P- and S-phases were spread widely under the volcano. In contrast, small shallow earthquakes observed near Showa-Shinzan did not display an apparent S-phase. These two characteristic earthquakes were called “A-type” and “B-type,” respectively, by Minakami et al. (1951).

Unlike the previous two eruptions, the eruption of 1977 occurred in the summit crater (Yokoyama et al., 1981). After only 36 hours of precursory felt earthquakes, a large dacitic ash column of the plinian type rose on the morning of August 7, 1977. More than ten eruptions, including four large ones, were repeated during the first week. During this beginning stage, numerous faults were found in the summit crater basin (Okada et al., 1981). At first, the major normal fault ran between the east side of Ko-Usu dome and Ogariyama, in a NW-SE direction. Then, the northeastern part was

uplifted and the fault developed into a large fault scarp (Fig. 2). Subsequently, two additional major normal faults were formed at both ends of the large fault, toward the northeast. These faults delineate a U-shaped fault zone where the uplift, as well as the thrust towards the northeast, is great. Additional normal faults, which run roughly parallel to the base of the U-shaped fault, formed graben (Okada et al., 1981). On November 16, 1977, phreatic explosions began around the uplifted area and continued for almost 11 months. Although explosions at the crater stopped in late October 1978, the blocky uplift of a new cryptodome inside the U-shaped fault and associated seismic swarm continued for almost four and a half years. The top of the uplifted area acquired a relative height of 180 m and was named Usu-Shinzan cryptodome. The seismicity under Usu volcano suddenly declined in March 1982. Repeated measurements using an electronic distance meter (EDM) and theodolite revealed that growth of the cryptodome had also stopped at the same time. Details of the activities and monitoring data for 1977–1982 were summarized by Okada et al. (1981), Yokoyama et al. (1981), and Yokoyama (1985).

In the afternoon of March 27, 2000, the number of small earthquakes under Usu volcano began to increase. Felt earthquakes occurred one day later, and then both occurrence frequency and magnitude increased until March 30, when surface ruptures were identified in the summit area and at the northwestern flank of the volcano. Eruption started at the northwestern foot in the afternoon of March 31 under a decreasing trend in the seismicity. Phreatic explosions continued for more than one and a half years at the newly opened craters. Localized uplift around the crater area continued for about four months and resulted in a new hill with a height of 70 m relative to the original topography. During the early phase of the 2000 eruption, uplift of the entire mountain centered at the southwestern crater was observed by theodolite, leveling, and GPS measurements (Mori and Ui, 2000).

Gravity changes before and after the beginning of the eruption suggested that shallow inflation and deep deflation sources were also located under the southwestern crater (Furuya et al., 2001). The large deformation at the northwestern flank before the initial eruption, which was observed by a quickly deployed GPS network, was recognized as a magma intrusion toward the new crater area (Okazaki et al., 2002). A quasi-vertical fissure toward the new crater area was suggested by gravity changes and GPS data (Jousset et al., 2003). The hypocenter distribution of precursory earthquakes was investigated using the three-dimensional (3D) velocity structure (Onizawa et al., 2007). After the initial phase showing vertical distribution, which lasted until March 28, the hypocenters spread horizontally north and south at depths of 2–3 km below sea level. No shallow earthquakes were found corresponding to magma intrusion in the uplifted area.

3. Previous studies on post- and inter-eruptive activities and underground structures

After the 1977–1982 eruption, Usu volcano became calm again at the surface. While the seismicity after March 1982 became very quiet (Fig. 3), rapid subsidence of Usu-Shinzan, the newly generated cryptodome, was observed by repeated EDM and theodolite measurements (Mori and Suzuki, 1998). The rate of subsidence in 1982–1997 relative to the southern crater rim was almost constant, at 40–60 mm/year (Fig. 4). The crater rim was also subsiding, with uniform subsidence at a rate of ~20 mm/year relative to the foot of the volcano. The subsidence was interpreted as contraction of the volcanic edifice after the 1977–1982 eruption. However, the amount of subsidence was very large, especially for Usu-Shinzan, which subsided about 0.8 m in 25 years, despite the baseline length of ~1000 m (Fig. 4 and Mori and Suzuki, 1998). The dome subsidence was also investigated by GPS and micro-gravity measurements (Jousset and Okada, 1998). Although measurements were only taken over a short time interval, the contraction of the volcano and the gravity increase around Usu-Shinzan were confirmed. The depth of the deflation source estimated by inversion analyses assuming a linear elastic medium was about 1000 m below sea level (Jousset and Okada, 1998).

Fumarole activities in and around the summit crater are still ongoing. The most vigorous fumarole is I crater (Fig. 1), which is located at the western foot of Usu-Shinzan. The fumarole temperature, as measured by the Sapporo District Meteorological Observatory of the Japan Meteorological Agency (JMA Sapporo), has gradually decreased from 700˚C to 350˚C since 1986 (Fig. 3). So far, the 2000 eruption has not affected fumarole activities at the summit in relation to the observed temperature.

Katsui et al. (1985) performed a topographic survey around the summit area to estimate the location of the magma that swelled Usu-Shinzan and discussed the magma intrusion process beneath Usu-Shinzan. Later, the magma body was clearly imaged at a depth of around sea level by magnetotelluric surveys (Matsushima et al., 2001, Ogawa et al., 1998). While a shallow part of the volcano to depths of 2–4 km is a conspicuous conductor (1–500 ・・m), a resistive block of 500–1000 Ωm is situated beneath Usu-Shinzan at depths of 300–500 m below sea level (Matsushima et al., 2001). The estimated extent of the intrusion is 600 m high and 300 m wide, which becomes 1.8×10^8 m^3 assuming that the intrusion is a 1000-m-long slab. The volume of intrusive magma was also estimated as 8×10^7 m^3 by integration of the heat discharge rate (Matsushima, 1993). Matsushima and Oshima (2000) investigated whether the intrusive magma can explain the thermal activities observed at the surface by a numerical simulation of the hydrothermal system. They confirmed that temporal change in heat discharge from Usu volcano can be explained by intrusive magma with initial temperature of 800˚C when the permeability of the magma is assumed to be about 10^{-13}–10^{-11} m^2 and that of the surrounding formation is assumed to be about 10^{-13} m^2, which is almost the same as the result of pumping tests at wells around Usu volcano. The

calculated temperature of the magma body was about 600˚C in 1990, which corresponds well with the decrease in fumarole temperature.

The fine-scale velocity structure around Usu volcano was investigated by Onizawa et al. (2002) using the precursory earthquakes of the 2000 eruption and by Onizawa et al. (2007) using artificial explosion signals. Although the spatial density of seismic stations was high enough for a tomography analysis to determine a 3D velocity structure with grid intervals of 2 km in horizontal directions, the intrusions of the 1977–1982 eruption and the 2000 eruption cannot be imaged from seismic waves.

4. Temporary seismic observation in 2006

4-1. Observation

We performed a temporary dense seismic observation in 2006 with the goal of revealing the precise hypocenter distribution and focal mechanisms of the shallow earthquakes under the summit crater. After the 2000 eruption, Usu Volcano Observatory, Hokkaido University, improved the seismic monitoring network for Usu volcano (Fig. 5a). Based on the continuous monitoring data obtained from this network, the main focal area is believed to be localized in the summit crater. To estimate the focal depth with a high degree of precision, temporary stations were deployed over the expected focal area. A total of 18 stations were installed on and around the summit crater and operated from June 7 to August 27, a period of about 80 days. Figure 5b shows the seismic stations used for the temporary observation plotted on an enlarged map of the summit area. The seismometers used at 10 of the 18 stations were Mark Products L4C-3D, and the remaining eight stations were equipped with Mark Products L22D (vertical component only). The signal outputs from the sensors were digitized by a Hakusan LS7000XT data converter, with 24 bit precision in continuous mode at 100 samples s^{-1} and were stored in a CF memory card. To avoid missing data, a radio telemetry system was installed for the SK01–SK09 summit stations, and the data were merged into the continuous monitoring data from the existing stations for real-time transmission to the observatory. Along with these temporary stations, seismic monitoring data were also provided from JMA Sapporo. Because the magnitudes of the volcanic earthquakes were small, data from the three close JMA stations were merged into our experimental data (Fig. 4b).

4-2. Triggering procedure

After integrating all of the seismic data, the event-detection processing was performed using the vertical component data from eight stations on the summit's crater or rim (SWRM, NRM, ERM, SRM, MSY, SK03, SK05, SK07). The threshold for the detection of seismic signals was that the averaged amplitude over a time window of 0.3 seconds had to exceed 2.0 to 3.0 times (depending on the site) that of the background noise. When two out of the eight stations satisfied the threshold, we judged that seismic signals had been observed during the time period. Under this condition, more than 6000 events were detected. For the detected data, manual selection was performed using the condition that a P-phase was identified for at least one existing station and that five or more P- or S-phase arrivals were determined. Finally, over 330 earthquakes were selected, and their hypocenters were estimated using a 1D velocity structure. This preliminary analysis had the goal of checking earthquake types and removing triggering errors. Most of the removed data were natural (bad weather) and artificial (fireworks and blasting) noises. The

selected earthquakes were the so-called A-type earthquakes having clear P- and S-phases; no low-frequency or long-period earthquakes (so-called B-type earthquakes) were recorded in this period.

4-3. Method of hypocenter relocation

To precisely estimate the hypocenter locations, we again selected earthquakes, this time under the conditions that five or more P-phase arrivals, five or more S-phase arrivals, and 15 or more total (the sum of P and S) arrivals were determined. The total number of earthquakes after this selection process was 142. Selection errors for the arrival times were set to be 0.03 s for P-phase and 0.05 s for S-phase arrivals, and their inverses were used for weighting the data in the relocation procedure. The width of selection errors roughly corresponded to the averaged worst uncertainty for the phase arrivals. Arrival data with larger uncertainty than these values were excluded from the dataset.

The three-dimensional P-wave velocity structure under Usu volcano was revealed by a seismic exploration using active sources in 2001 (Onizawa et al., 2007). In this study, we used the estimated P-wave structure and an S-wave structure constructed from the P-wave structure, assuming the relation Vp = 1.45 Vs + 0.9, as estimated by Onizawa et al. (2007). Using this relation, for example, Vs = 0.76 km/s and Vp/Vs = 2.64 at the area of Vp = 2.0 km/s, and Vs = 3.51 km/s and Vp/Vs = 1.71 at the area of Vp = 6.0 km/s. The depth dependency of the Vp/Vs ratio hardly constrains the result of the relocation analysis here because most earthquakes under the volcano are distributed in shallow areas and have short time intervals for the P- and S-phases. Because the assumed S-wave velocity structure is uncertain relative to the P-wave structure, we performed a comparative relocation analysis, assuming Vp/Vs = 1.73 in some cases. Hereafter, we describe these velocity models as the “linear model” and “constant model,” respectively.

The hypocenter locations determined in this analysis depended on the initial value. To check the dependencies, the initial hypocenter locations were distributed on grids set over the entire volcano. This process confirmed that the relocation results were independent of the initial value.

4-4. Spatial distribution of hypocenters

Except for three deep earthquakes with depths of >1 km below sea level, all the events were distributed in a shallow area under the summit crater. Figure 6 shows the distribution of 142 earthquakes, which were relocated using the linear model. Shallow earthquakes were extremely localized at depths of 1 km or less.

Focusing on the shallow activity of 139 earthquakes, we performed the relocation analysis

again, setting a fine distribution for the initial hypocenters. The maximum and minimum magnitudes were 1.9 and –1.4, respectively. Seven dominant earthquakes with magnitudes larger than 1.0 were identified. Figure 7 presents a close-up view of the summit area. The standard deviations in the relocation errors for the hypocenters were 50 m or less in the horizontal direction and 100 m or less in the vertical direction. When we used the constant model, the average depth shifted downward about 174 m, even though the epicenters were in almost the same positions. The averaged travel-time residual of the S-wave of the linear model was a negative value of –0.121 s, whereas that of the constant model became a positive value of 0.083 s. This result indicated that the synthetic travel times of the S-wave for the linear model were longer than the observed ones. That is, the assumed S-wave velocity was too slow relative to the P-wave velocity. On the other hand, the S-wave velocity was too fast for the constant model. Therefore, the Vp/Vs ratio between the “linear” and “constant” models would be adequate for shallow earthquakes. Because the differences in the hypocenters between these two models were only in the vertical direction, the hypocenters were expected to be distributed at an intermediate depth between the linear model and the constant model when we used an adequate Vp/Vs ratio.

As seen in Fig. 7, micro-earthquakes occurring in the summit crater were localized in the southwestern part of the crater at a range of 200–600 m below sea level. They were distributed in the southwestern foot of Usu-Shinzan cryptodome, which was newly created in the 1977–1982 eruption. The focal area can be divided into three clusters: near I crater (cluster “IC” in Fig. 7), near Ginnuma crater (cluster “GC” in Fig. 7), and east of Ginnuma crater (cluster “GE” in Fig. 7) (see also Fig. 1). In the plane view, the hypocenters show a bowl-shaped opening toward the northeast.

The spatiotemporal distribution of the hypocenters during the experiment is presented in Fig. 8. The most active focal area was GC, at which 99 earthquakes occurred during the experiment, including four of the seven dominant earthquakes. Although the seismicity seemed steady, high activity periods (around June 10, late July, and mid-August) and low ones (mid-July and early August) were observed. This fluctuation was not correlated with rainfall. The seismicity of clusters IC (22 events) and GE (16 events) was relatively low, about one-fifth of that of GC. The difference in the number of earthquakes reflects the actual seismicity because these focal areas were densely covered by the temporarily deployed seismic stations.

4-5. Estimation of focal mechanisms

An estimation of the focal mechanism gives us meaningful information about crustal activity. Because the magnitudes of the earthquakes were very small and the earthquakes were A-type, we assumed a double-couple mechanism and determined the focal mechanisms of the seven

dominant earthquakes using the P-wave polarities estimated by the relocation analysis in the previous section. A grid-search procedure was adopted that changed the direction of the principal axes at an interval of 5 degrees. The estimated mechanisms are plotted in Fig. 9 using upper-hemisphere projection.

All of the estimated mechanisms commonly have a steep-dipping nodal plane and a nearly horizontal plane. As for the four dominant earthquakes in cluster GC, the steep-dipping planes are directed almost east and west. Because we plotted the focal mechanisms in Fig. 9 using upper-hemisphere projection, these mechanisms represent the subsidence of the northern block relative to the southern side, if we assume a steep-dipping plane as a fault plane. The mechanisms of the two earthquakes belonging to cluster GE suggest subsidence of the northwestern side because strikes of the steep-dipping plane of the two earthquakes in cluster GE are roughly directed northeast and southwest. The largest earthquake (M 1.9) in cluster IC has a large dip-slip component indicating subsidence of the eastern side. Roughly speaking, the alignment of the clusters and the focal mechanisms suggest the subsidence of the northeastern side of the focal clusters.

The hypocenters of the four earthquakes in cluster GC are distributed in proximity to each other. If these events repeatedly occurred on the same fault plane, the same mechanisms and similar waveforms would be expected. However, the polarity distribution on the focal sphere and the estimated mechanisms of the four earthquakes in cluster CG differ somewhat (Fig. 9). The waveforms of these four events are also different, as illustrated by the example shown in Fig. 10.

Although the actual fault plane cannot be uniquely determined by the focal mechanisms shown in Fig. 8, we assume that the steep-dipping plane is the fault plane because long-term subsidence around Usu-Shinzan cryptodome has been observed by EDM and theodolite measurements, as introduced in section 3. Cryptodomes (US and OG in Fig. 9) are located on the northeastern side of the seismic clusters revealed in this study. The focal mechanisms strongly suggest that the shallow seismic activities are associated in some way with the successive cryptodome subsidence.

5. InSAR analysis and GPS measurements

Subsidence of lava domes and cryptodomes has been observed by repeated physical measurements since the 1977–1982 eruption. In the 1990s, the subsiding rate at Usu-Shinzan was 40–50 mm/year (Mori and Suzuki, 1998). The spatial distribution of the subsiding area was investigated by the Geographical Survey Institute (Yarai et al., 2000) using SAR data from the Japanese Earth Resources Satellite-1 (JERS-1). An interferogram made from the images acquired by JERS-1 on October 15, 1992, and May 1, 1998, revealed that the subsidence was centered at the O-Usu lava dome, on the eastern half of the summit crater.

To investigate the current rate of subsidence and the spatial distribution of the surface deformation, InSAR analysis and temporary GPS measurement were performed. Because these two measurements are independent, we can confirm that the atmospheric effect usually associated with topography is adequately excluded from the result of the InSAR analysis by comparing the deformation rate at specific locations where GPS measurements were performed. Descending images from the Advanced Land Observing Satellite (ALOS) with an off-nadir angle of 41.5˚taken on July 23, 2006, and October 26, 2007, (interval of 460 days) were used for the interferometry analysis. The topographic effect was removed by using a 10-m-resolution digital elevation model (DEM) supplied by the Geographical Survey Institute (GSI). Ground deformation away from the satellite can be seen at the summit area and the uplifted area of the 2000 eruption (Fig. 11), reflecting the subsidence or contraction of the ground at these areas. This feature is universal for interferograms using different image pairs.

Temporary GPS measurements were performed on November 7, 2006, and May 7, 2008, (interval of 547 days) almost overlapping with the SAR data acquisition. In addition to the two continuous GPS stations, six points were located. Figure 11 plots the movements of GPS stations relative to the reference point IRE. Subsidence was dominant around the summit crater, and a maximum depression of more than 40 mm was observed at USS, located on Usu-Shinzan cryptodome. In contrast, CHO on the southern side of the volcano showed almost no movement. This suggests that the subsiding area is very small and restricted to an area near the summit crater. Horizontal displacements indicate the plane contraction of the summit area. Three stations on the southwestern rim not only subside but also move toward the east-northeast. Two stations on the northern side, USS and NRM, moved toward the east-southeast, and OUY moved to the northwest. Therefore, these results strongly suggest that not only subsidence of domes but also horizontal contraction at the summit area is in progress.

The GPS measurements give us authoritative information about the spatial distribution of the deformation. The subsiding area seen in the interferogram is slightly shifted eastward, as if O-Usu lava dome were the centroid. Because of the radar beam direction, looking westward

down from the satellite, the variation due to contraction and subsidence is emphasized at the eastern side of the volcano. In fact, little change is seen around the three stations on the southwestern rim in the interferogram, although the GPS measurements captured the subsidence and east-northeastward motion. The eastward horizontal motion apparently compensates for the subsiding motion in the SAR image because the resulting motion is tangential to the radar beam. The fact that ground deformation at the southwestern rim was not seen in the interferogram but was obviously detected by GPS analysis ensures that the fringe in the interferogram is independent of a topography-related atmospheric effect. Therefore, it is reasonable to conclude that the centroid of subsidence is located near USS, Usu-Shinzan cryptodome, as suggested by the GPS analysis. The consistency of the subsiding rates estimated by GPS and InSAR analyses was confirmed by calculating changes in the line of sight (ΔLOS) of the radar at the GPS stations (Table 1). To compare these values, the ΔLOS of the InSAR analysis was converted to a rate for an interval of 547 days. The ΔLOS of InSAR agrees well with that of the GPS, to within a few millimeters, except for two sites. The error at two sites probably arose from an artificial problem involving operation of a GPS receiver.

The fringe around the summit crater is restricted to a small area, less than 2 km in diameter. Figure 12 shows temporal change in slant range along two lines with the cross-sectional topography. The figure illustrates remarkable subsidence inside the crater. Large steps are evident in the range change on both sides of the summit lava domes in line 1, which suggest that the domes are subsiding more rapidly than the surrounding area. The range change along line 2 also shows localized deformation at the summit area. Because the shapes of the ΔLOS line and cross-sectional topography are different, we consider the atmospheric effect to have been adequately removed from the interferogram.

6. Discussion

6-1. Focal mechanisms and surface deformation

It is noteworthy that the seismic activity is localized along the U-shaped fault created in the 1977–1982 eruption and that focal mechanisms suggest the subsidence of the Usu-Shinzan cryptodome that stands at the inner side of the U-shaped fault. The InSAR and GPS analyses also confirm that dome subsidence is still continuing. The results from seismic and geodetic studies are very consistent in terms of the dome subsidence and suggest that the micro-earthquakes along the U-shaped fault closely correlate with ground deformation.

The significant features of the seismicity in the 1977–1982 eruption were the correspondence to crustal deformation (e.g., Harada et al., 1978, Takeo, 1983) and the existence of groups of earthquakes with similar waveforms (e.g., Okada et al., 1981, Nishimura and Okada, 1987). Using quasi-continuous EDM measurements, Harada et al. (1978) found that the occurrence of large earthquakes coincided well with the stepwise progression of crustal deformation associated with dome growth. Takeo (1983) also quantitatively confirmed that the cumulative slip distance at the dome wall estimated from seismic wave analysis was consistent with the amount of cryptodome growth determined from geodetic measurements. The results of these previous studies suggest the stepwise subsidence associated with volcanic earthquakes. According to previous studies on scaling laws for fault slips, the fault radius is 100–300 m, and the amount of slip is several to tens of millimeters for an M~1 earthquake (e.g., Haar et al., 1984, Takeo, 1983), which corresponds to the magnitude of the major earthquakes in 2006. Because the seismicity of Usu volcano is steady on a long time scale (Fig. 8), the annual number of M~1 class earthquakes in the most active cluster GC becomes 16 (four events were observed over approximately three months). If we assume that all major earthquakes occur on the same fault plane, rough estimation of total slip amount associated with a major earthquake can be obtained by a simple summation. Letting the typical amount of slip for an M~1 earthquake be 2 mm, the annual slip rate will be about 30 mm per year, which is comparable to the subsiding rate of Usu-Shinzan cryptodome. However, as indicated in section 4-5, the M~1 earthquakes differed somewhat in their focal mechanisms, despite the proximity of their hypocenters. This fact suggests that these four major earthquakes were excited by different fault planes. Therefore, the total slip rate of 20 mm per year may be overestimated. Because calculation of the amount of fault slip from magnitude includes large uncertainty, the values shown here are only a rough indication, and we cannot conclude how the earthquakes contribute to the cryptodome subsidence. Even so, it is strongly suggested that the earthquakes closely relate to the physical process of the subsidence.

The hypocenter distributions of the dome-growth earthquakes are plotted in Fig. 9 with pink

and blue dots. The earthquakes in October 1977 (432 events having two or more similar earthquakes) are shown by pink dots and those in April 1978 (268 events, same as above) are shown by blue dots. This figure is a modified plot of Figure 2 by Nishimura and Okada (1987). Such a direct comparison may be inadequate because their analysis used a uniform velocity structure of Vp = 3.0 km/s, which is different from our 3D velocity model. However, it is sufficient to understand the rough spatial relationship. The focal cluster IC almost corresponds to the pink dots, which is a focal cluster for October 1977, and the cluster GC almost overlaps the blue dots. Although the four dominant earthquakes belong to the same focal cluster GC, the waveforms and spatial distributions of P-wave polarity differ slightly among these events (Figs. 9 and 10). The waveform similarities of volcanic earthquakes during an inter-eruptive period will be investigated in detail in a future study.

Since the epicenter distribution in 2006 almost overlaps that for the 1977–1982 activity, a comparison of focal mechanisms is worthwhile. Harada (1981) estimated the focal mechanisms of volcanic earthquakes during the building stage of Usu-Shinzan in 1977–1979. Figure 13 presents the averaged mechanisms for each group of similar earthquakes (modified from Fig. 3 (f) of Harada, 1981). Among the seven earthquakes analyzed in this study, the events in cluster IC were located near cluster 11 in Fig. 13, and the focal mechanisms of eastward and down dip-slip are quite similar. The events in cluster GC correspond approximately to cluster 10 in Fig. 13, but their focal mechanism is similar to that of cluster 9, which had a northward and downward dip-slip mechanism. The events in cluster GE are spatially close to cluster 9 in Fig. 13. However, the fault azimuths are different; the fault plane was directed northeast and southwest in 2006, which is almost parallel to the eastern edge of the U-shaped fault, although Harada (1981) reported that fault to run east and west. To compare the focal mechanisms and spatial distribution of the hypocenters in detail, further acquisition of seismic data and statistical processing is required.

6-2. Interpretation of the crustal activity under the summit crater

As noted in section 3, after the 1977–1982 eruption, seismic activity of Usu volcano remained at a low level. It began increasing around 1995, which was five years before the last eruption. As the monthly frequency of earthquakes under the volcano gradually increased until the eruption, earthquake frequency may be regarded as a long-term precursor. However, the seismicity did not return to the pre-1995 level even with the termination of the magmatic eruption in 2000. This fact represents a difficulty for considering earthquake frequency as a precursor.

During the dome-growth period, the U-shaped fault was seismically active because the

growth rate of the dome (i.e., strain rate around the U-shaped fault) was high enough to excite earthquakes. In the early stage of the 1977–1982 eruption, focal clusters near I crater and Ginnuma crater were most active (NK and SK blocks in Fig. 4 of Okada et al. 1981). The seismicity of these two clusters decreased within one year, and the focal area moved northeastward along the U-shaped fault. Soon after the termination of the 1977–1982 eruption, subsidence of Usu-Shinzan cryptodome began, coincident with a decrease in the number of earthquakes. The deformation rate of the subsidence was 1/100 or less compared to that of uplift (Mori and Suzuki, 1999). The monthly frequency of volcanic earthquakes also reached almost 1/100 in February through September 1982 (Yokoyama, 1985). Because dome growth had continued over four and a half years, the thermal condition around the focal area can be regarded as having been in a steady state during the transition from uplift to subsidence. Therefore, the decrease in the number of earthquakes is suggested to reflect a strain rate change around the U-shaped fault. However, the gradual increase in seismicity since 1995 cannot be explained by the same logic because the dome subsidence rate is almost stable. Unfortunately, we do not know the precise locations of the hypocenters of volcanic earthquakes before the 2000 eruption because of a lack of seismic stations. Since the S-P times of shallow volcanic earthquakes before and after the 2000 eruption are almost the same, we can expect that the focal area after 1995 was distributed in a similar location to that in 2006.

From the viewpoint of long-term volcanic activity, significant changes over time in monitoring data were dome subsidence and decrease in fumarole temperature. Dome subsidence and temperature decrease were unidirectional phenomena. A candidate for the cause of seismic re-activation is cooling of intrusive magma under Usu-Shinzan. The temperature dependency of friction has been confirmed by laboratory experiments for wet fault gouge (Blanpied et al., 1991). Generally speaking, a fault slips intermittently and causes earthquakes at low ambient temperature, but at high temperature, the fault moves aseismically. When the intrusion began in 1977, the surrounding rock was kept at low temperature. Earthquakes occurred in the vicinity of the intrusive magma, where the strain rate was maximal due to the intrusion. The focal area near the intrusion was then heated by the magma, and the rock temperature exceeded an upper limit of stick slips. The decrease of seismicity near I crater and Ginnuma crater in summer 1978 may have been related to such heating. Soon after the 1977–1982 eruption, fumarole temperature at I crater reached 700˚C, which is high enough for aseismic creeping, as introduced in section 3. Reactivation of volcanic earthquakes from 1995 can be explained by the reverse process. According to the result of numerical simulation of hydrothermal activity by Matsushima and Oshima (2000), the temperature of the magma body that intruded beneath Usu-Shinzan may have decreased to about 600˚C in 1990. The extent of the heated zone around the magma was calculated to be restricted to about 100 m in the

horizontal direction.

For the surface to subside, volume decrease must occur under the ground. Jousset and Okada (1999) performed GPS and microgravity measurements at Usu volcano in 1996 and 1997 and quantitatively discussed the effect of devesiculation and cooling of intrusive magma to explain dome subsidence and gravitational change. Devesiculation may play a key role in the volume decrease under Usu-Shinzan because four large eruptions in August 1977 ejected large amounts of pumice. However, we cannot conclude what controls the dome subsidence from the limited data obtained in 2006.

Finally, we present a schematic image for the shallow crustal activities of Usu volcano (Fig. 14). The magma of the 1977–1982 eruption reached a depth of a few hundred meters below the surface. The present seismic activities and surface deformation are strongly related to the cooling of the magma under Usu-Shinzan. Since the 1977–1982 eruption spewed a large amount of pumice, the dome subsidence after the eruption may be explained by contraction and passive degassing, as suggested by Jousset and Okada (1999). In the 2000 eruptive period, magma rose from a deep area 4–6 km below sea level (Tomiya and Miyagi, 2002, Yamamoto et al., 2002) under the southwestern part of the summit crater. In the case of the flank eruption, the magma stagnated at a certain depth, at around 2 km below sea level, as revealed by seismic and geodetic studies of the 2000 eruption (Furuya et al., 2001, Onizawa et al., 2007). This magma then migrated obliquely upward along the surface of equal density (Onizawa et al., 2007). This schematic model should be confirmed and improved by multi-parameter monitoring. Additional information on gravity changes and magnetic monitoring will be required to discuss the cooling, contraction, and degassing of the intrusive magma in detail.

7. Conclusion

The inter-eruptive volcanism of Usu volcano was investigated by seismic and geodetic analyses. Although flank eruption occurred in 2000, seismic activity under the summit crater has continued since 1995. The focal areas are distributed along the U-shaped fault that surrounds Usu-Shinzan cryptodome, which developed during the 1977–1982 summit eruption. The focal mechanisms of the dominant earthquakes indicate subsidence of the inner side of the U-shaped fault. InSAR analysis and GPS measurements revealed blocky and localized subsidence around Usu-Shinzan cryptodome. The current rate of subsidence at Usu-Shinzan is about 30 mm/year. The findings suggest that earthquakes along the U-shaped fault are closely related to the dome subsidence deformation. The reactivation of seismicity from 1995 may be explained by the cooling of intrusive magma under Usu-Shinzan.

We have proposed a schematic model for the crustal activity of Usu volcano. This model includes and is consistent with results of past studies. The model proposed in this paper must be modified and improved in the future to understand the post- and inter-eruptive volcanism of Usu volcano. For mid- to long-term eruption predictions, comprehensive monitoring of the crustal activity will be important.

Acknowledgements

Discussions about volcano deformation and analysis techniques with Dr. Y. Aoki were very fruitful (H.A.). The authors especially thank all of the staff members of the Volcanic Observations and Information Center, Sapporo District Meteorological Observatory, Japan Meteorological Agency, for providing the earthquake catalog and data on fumarole temperatures. We are also grateful to the two anonymous reviewers who helped us to improve this manuscript. Some instruments for seismic observation were supported by the Sakurajima Volcano Research Center, Disaster Prevention Research Institute (DPRI), Kyoto University; Volcano Research Center, Earthquake Research Institute (ERI), University of Tokyo; and Hakusan Corporation. PALSAR level 1.0 data were shared by the PALSAR Interferometry Consortium to Study Our Evolving Land Surface (PIXEL), and provided from the Japan Aerospace Exploration Agency (JAXA) under a cooperative research contract with ERI, University of Tokyo. The PALSAR data are owned by the Ministry of Economy, Trade and Industry (METI) and JAXA. Maps were drawn using GMT software (Wessel and Smith, 1991).

References

Blanpied, M. L., Lockner, D. A., Byerlee, J. D., 1991. Fault stability inferred from granite sliding experiments at hydrothermal conditions. Geophys. Res. Lett. 18: 609 – 612.

Briole, P., Massonnet, D., Delacourt, C., 1997. Post-eruptive deformation associated with the 1986–87 and 1989 lava flows of Etna detected by radar interferometry. Geophys. Res. Lett. 24: 37 – 40.

Dzurisin, D., Poland, M. P., Burgmann, R., 2002. Steady subsidence of Medicine Lake volcano, northern California, revealed by repeated leveling surveys. J. Geophys. Res. 107: doi:10.1029/2001JB000893.

Furuya, M., 2004. Localized deformation at Miyakejima volcano based on JERS-1 radar interferometry: 1992–1998. Geophys. Res. Lett. 31: doi:10.1029/2003GL019364.

Furuya, M., Ohki, Y., Okubo, S., Maekawa, T., Oshima, H., Shimizu, H., 2001. Urgent gravity measurements for the eruption of Usu volcano in 2000 – construction of absolute gravity network and the co-eruptive and post-eruptive gravity changes. Bull. Earthq. Res. Inst. Univ. Tokyo 76: 237 – 246 (in Japanese with English abstract).

Harada, T., 1981. Stress field in Usu volcano deduced from focal mechanism solutions. Bull. Volcanol. Soc. Japan 26: 93 – 110 (in Japanese with English abstract).

Harada, T., Yamashita, H., Watanabe, H., 1979. Quasi-continuous observation of changes in distance caused by the 1977 – 1978 eruption of Usu volcano, Hokkaido. Geophysical Bulletin of Hokkaido University 38: 31 – 40 (in Japanese with English abstract).

Jousset, P., Okada, H., 1999. Post-eruptive volcanic dome evolution as revealed by deformation and microgravity observations at Usu volcano (Hokkaido, Japan). J. Volcanol. Geotherm. Res. 89: 255 – 273.

Jousset, P., Mori, H., Okada, H., 2003. Elastic models for the magma intrusion associated with the eruption of Usu Volcano, Hokkaido, Japan. J. Volcanol. Geotherm. Res., 125: 81 – 106.

Katsui, Y., Komuro, H., Uda, T., 1985. Development of faults and growth of Usu-Shinzan Cryptodome in 1977 – 1982 at Usu Volcano, north Japan. J. Fac. Sci., Hokkaido Univ., Ser. IV 21: 339 – 362.

Lu, Z., Masterlark, T., Dzurisin, D., 2005. Interferometric synthetic aperture radar study of Okmok volcano, Alaska, 1992–2003: magma supply dynamics and postemplacement lavaflow deformation. J. Geophys. Res. 110: doi:10.1029/2004JB003148.

Lu, Z., Masterlark, T., Power, J., Dzurisin, D., Wicks, C., 2002. Subsidence at Kiska Volcano, Western Aleutians, detected by satellite radar interferometry. Geophys. Res. Lett. 29: doi:10.1029/2002GL014948.

Matsushima, N., 1993. Geothermal activity associated with the 1977 eruption of Usu volcano. Chishitsu News, 466, 25-32 (in Japanese).

Matsushima, N., Oshima, H., 2000. Numerical simulation of geothermal activity associated with the 1977 eruption of Usu volcano. Report to the Ministry of Education, Science, Sports and Culture for 1997 – 1999 Grant-in-Aid for Scientific Research (no. 09640498): 19 – 30 (in Japanese).

Matsushima, N., Oshima, H., Ogawa, Y., Takakura, S., Satoh, H., Utsugi, M., Nishida, Y., 2001. Magma prospecting in Usu volcano, Hokkaido, Japan, using magnetotelluric soundings. J. Volcanol. Geotherm. Res. 109: 263 – 277.

Minakami, T., Ishikawa, T., Yagi, K., 1951. The 1944 eruption of Volcano Usu in Hokkaido, Japan. Bull. Volcanol., Ser. II 11: 45 – 157.

Mori, H. Y., Suzuki, A., 1998. Volcanic ground deformation at Mt. Usu – a perspective of the deformation in the last twenty years. Geophysical Bulletin of Hokkaido University 61: 275 – 285 (in Japanese with English abstract).

Mori, H. Y., Ui, T., 2000. Crustal deformation and eruptic activities of Mt. Usu in 2000. J. JSNDS 19: 383 – 390 (in Japanese with English abstract).

Nishimura, Y., Okada, H., 1987. Detailed structure of volcanic earthquake concentration at Mt. Usu in 1977 – 1978. Geophysical Bulletin of Hokkaido University 49: 23 – 30 (in Japanese with English abstract).

Ogawa, Y., Matsushima, N., Oshima, H., Takakura, S., Utsugi, M., Hirano, K., Igarashi, M., Doi, T., 1998. A resistivity cross section of Usu volcano, Hokkaido, Japan, by audiomagnetotelluric soundings. Earth Planets Space 50: 339 – 346.

Okada, Hm., Watanabe, H., Yokoyama, I., 1981. Seismological significance of the 1977 – 1978 eruptions and the magma intrusion process of Usu volcano, Hokkaido. J. Volcanol. Geotherm. Res. 9: 311 – 334.

Okazaki, N., Takahashi, H., Kasahara, M., Ishimaru, S., Mori, H. Y., Kitagawa, S., Fujiwara, K., Churei, M., 2002. Crustal deformation associated with the 2000 eruption of Usu volcano as observed by a dense GPS array. Bull. Volcanol. Soc. Japan 47: 495 – 506 (in Japanese with English abstract).

Omori, F., 1911. The Usu-san eruption and earthquakes and elevation phenomena. Bull. Imp. Earthq. Invest. Comm. 5: 1-38.

Onizawa, S., Oshima, H., Mori, H. Y., Maekawa, T., Suzuki, A., Ichiyanagi, M., Okada, H., 2002. Three-dimensional seismic velocity structure around Usu volcano, Japan. Bull. Volcanol. Soc. Japan 47: 495 – 506 (in Japanese with English abstract).

Onizawa, S., Oshima, H., Aoyama, H., Mori, H. Y., Maekawa, T., Suzuki, A., Tsutsui, T., Matsuwo, N., Oikawa, J., Ohminato, T., Yamamoto, K., Mori, T., Taira, T., Moyamachi, H., Okada, H., 2007. P-wave velocity structure of Usu volcano: Implication of structural controls on magma movements and eruption locations. J. Volcanol. Geotherm. Res. 160: 175 – 194.

Simkin ,T., Siebert, L., 2000. Earth's volcanoes and eruptions: an over view. In: H. Sigurdsson

(Editor-in-Chief), Encyclopedia of volcanoes. Academic Press, San Diego, CA, pp. 249 – 261.

Stevens, N. F., Wadge, G., Williams, C. A., Morley, J. G., Muller, J. P., Murray, J. B., Upton, M., 2001. Surface movements of emplaced lava flows measured by synthetic aperture radar interferometry. J. Geophys. Res. 106: 11293 – 11313.

Takeo, M., 1983. Source mechanisms of Usu volcano. Japan, earthquakes and their tectonic implications. Phys. Earth Planet. Inter. 2: 241 – 264.

Tomiya, A., Miyagi, I., 2002. The eruptive products and magma process of March 31, 2000 eruption of Usu volcano. Bull. Volcanol. Soc. Japan 47: 663 – 673 (in Japanese with English abstract).

Wessel, P., Smith, W. H. F., 1991. Free software helps map and display data. EOS Trans. AGU 72: 441.

Yarai, H, Murakami, M., Tobita, M., Nakagawa, H., Ozawa, S., Sagiya, T., Nishimura, T., Fujiwara, S, 2000. Crustal deformation on and around Usu volcano before the 2000 eruption by JERS-1 SAR interferometry. Fall Meeting Abstract, The Volcanological Society of Japan: A43. (in Japanese)

Yamamoto, M., Kawakatsu, H., Yomogida, K., Koyama, J., 2002. Long-period (12 sec) volcanic tremor observed at Usu 2000 eruption: Seismological detection of a deep magma plumbing system. Geophys. Res. Lett. 29: doi:10.1029/2001GL013996.

Yokoyama, I., 1985. Volcanic processes revealed by geophysical observation of the 1977 – 1982 activity of Usu volcano, Japan. J. Geodynamics, 3: 351 – 367.

Yokoyama, I., Yamashita, H., Watanabe, H., Okada, Hm., 1981. Geophysical characteristics of dacite volcanism. The 1977 – 1978 eruption of Usu volcano. J. Volcanol. Geotherm. Res. 9: 335 – 358.

Yokoyama, I., Katsui, Y., Oba, Y., Ehara, S., 1973. Usu-zan, its volcanic geology, history of eruption, present state of activity and prevention of disaster. Committee for Prevention of Disasters of Hokkaido, Sapporo, pp. 1–254 (in Japanese).

Figure Captions

Fig. 1 Lava domes, upheavals, and eruptive craters of Usu volcano. The contour interval of the topography is 50 m.

Fig. 2 Aerial photograph of Usu volcano taken by the Geographical Survey Institute in 1979. Because the summit crater is free of vegetation, the topography is clearly visible. Abbreviations indicate the locations of reference peaks of the summit domes; O-Usu (OU), Ko-Usu (KO), Ogariyama (OG), and Usu-Shinzan (US). These four points are used as common references in the following figures. The dashed line depicts the surface trace of the U-shaped fault.

Fig. 3 Temporal change in fumarole temperature of I crater and monthly frequency of volcanic earthquakes of Usu volcano. Original data were provided by the Sapporo District Meteorological Observatory, Japan Meteorological Agency. Gray shading denotes eruptive periods in 1977–1982 and in 2000. The threshold amplitude for counting earthquakes changed in August 1994.

Fig. 4 Temporal changes in the altitude of benchmarks established on the summit domes. The reference point of the EDM measurement was SRM. Abbreviations of the benchmarks are the same to those in Fig. 2. Discontinuity in the graph denotes replacement of benchmarks on the domes.

Fig. 5 (a) Map view of continuously operated seismic stations around Usu volcano. The contour interval of the topography is 100 m. Double circles and single circles express three-component and single-component stations, respectively. Circles with a cross show non-operating stations during the temporary observations in 2006. (b) Map of stations engaged in temporary seismic observations in 2006. The contour interval of the topography is 50 m. The area corresponds to the rectangle with the broken line in (a). The double circle, single circle, and circle with cross are the same as in (a). Open squares depict temporary stations installed by Hokkaido University. Open triangles show continuously operated stations of the Sapporo Meteorological Observatory, Japan Meteorological Agency. The three-component stations are SK01, SK03, SK05, SK07, SK10, SK12, Sk13, SK16, SK18, SK19, JMAA, and GNTG. The single-component stations are SK02,

SK04, SK06, SK08, SK09, SK11, SK14, SK15, and KBBY. Solid triangles indicate reference peaks of the summit domes (see Fig. 2).

Fig. 6 Hypocenter map for the 142 selected events. The contour interval of the topography is 100 m. Crosses indicate the locations of seismic stations. The three-dimensional P-wave velocity model is underlain in the EW and NS cross sections. OU and KU indicate reference peaks of the summit domes (see Fig. 2).

Fig. 7 Hypocenter map for the 139 events that occurred beneath the summit crater. The contour interval of the topography is 50 m. Crosses indicate the locations of seismic stations. Solid triangles mark reference peaks of the summit domes (see Fig. 2). IC, GN, and EG indicate the focal clusters near I crater, beneath Ginnuma crater, and east of Ginnnuma, respectively.

Fig. 8 Spatiotemporal distribution of volcanic earthquakes during the temporary observation in 2006. The top graph shows the cumulative number of earthquakes under the summit crater. The hypocenter list of the 139 relocated earthquakes is used for this figure.

Fig. 9 Hypocenter location map of relocated earthquakes and focal mechanisms of seven major earthquakes with magnitude larger than 1.0. Focal mechanisms are shown by upper-hemisphere projection. Pink and blue dots overlaid on the map express hypocenters in October 1977 and in April 1978, respectively (Original plot was given by Nishimura and Okada, 1987). Thick lines express the crater rim and the U-shaped fault. IC, GN and EG indicate the three focal clusters as in Fig. 7.

Fig. 10 Waveforms of four major earthquakes belonging to the focal area beneath Ginnuma crater. These data were vertical components recorded at ERM.

Fig. 11 Interferogram of an SAR image of Usu volcano area. The images were acquired by ALOS on July 23, 2006, and October 26, 2007. Red circles mark the locations of GPS measurement points. The reference point of the GPS analysis is IRE. Horizontal and vertical motions are expressed by

black arrows and bars, respectively.

Fig. 12 Slant range change along two lines crossing the summit. Cross-sectional lines A–B and C–D are shown by the interferogram.

Fig. 13 Averaged fault mechanisms of volcanic earthquakes during the 1977–1982 eruption period estimated by Harada (1981). Gray-shaded areas express focal areas of earthquake families having similar waveform. This figure was modified from Fig. 3f of Harada (1981).

Fig. 14 Cross-sectional image of crustal activity under Usu volcano. Cross-sectional lines are shown in the map view at the bottom right (A–B and C–D). Graphs at the top show slant range changes along the lines (see Fig. 12). The focal area of the inter-eruptive volcanic earthquakes determined in this study is located at 0–0.5 km below sea level, which is shown by thick black ovals. The projected focal mechanism is overlaid on the cross section. The depth range of the shallower magma chamber was estimated from petrological study at 4–6 km below sea level (Tomiya and Miyagi, 2002). The inflation and deflation sources for the 2000 eruption were estimated to be 2 km and 3 km below sea level, respectively (Furuya et al., 2001). The hypocenters of the precursory earthquakes of the 2000 eruption were mainly located at depths of 2–3.5 km below sea level (Onizawa et al., 2007). The shallow intrusion of magma during the 1977–1982 eruption was estimated under Usu-Shinzan by magnetotelluric surveys (Ogawa et al., 1998, Matsushima et al., 2001).

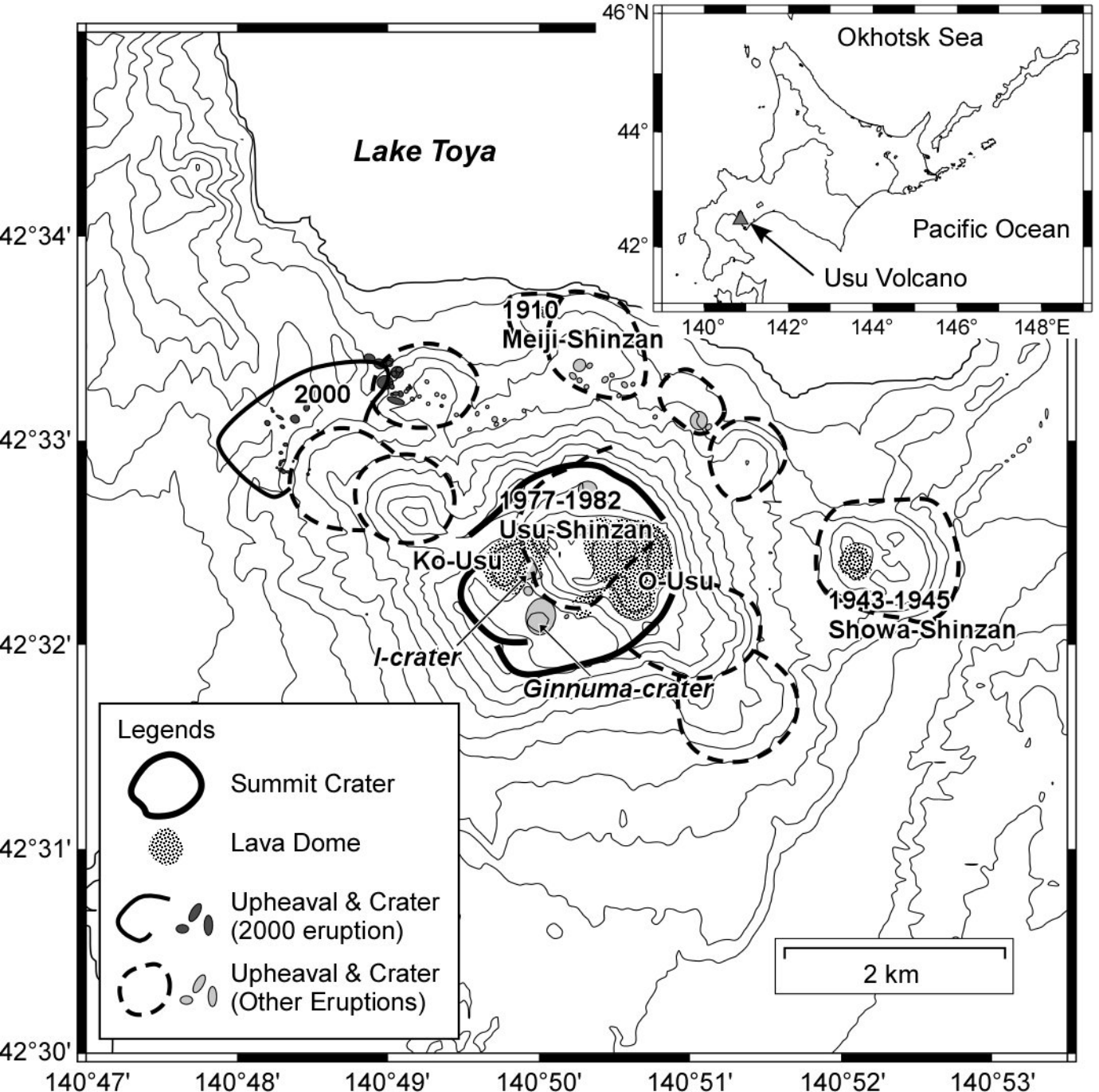
Lake Toya
Okhotsk Sea
Pacific Ocean
Usu Volcano
46°N
44°
42°
140°
142°
144°
146°
148°E
1910
Meiji-Shinzan
2000
1977-1982
Usu-Shinzan
Ko-Usu
O-Usu
1943-1945
Showa-Shinzan
I-crater
Ginnuma-crater
Legends
Summit Crater
Lava Dome
Upheaval & Crater
(2000 eruption)
Upheaval & Crater
(Other Eruptions)
2 km
42°34'
42°33'
42°32'
42°31'
42°30'
140°47'
140°48'
140°49'
140°50'
140°51'
140°52'
140°53'

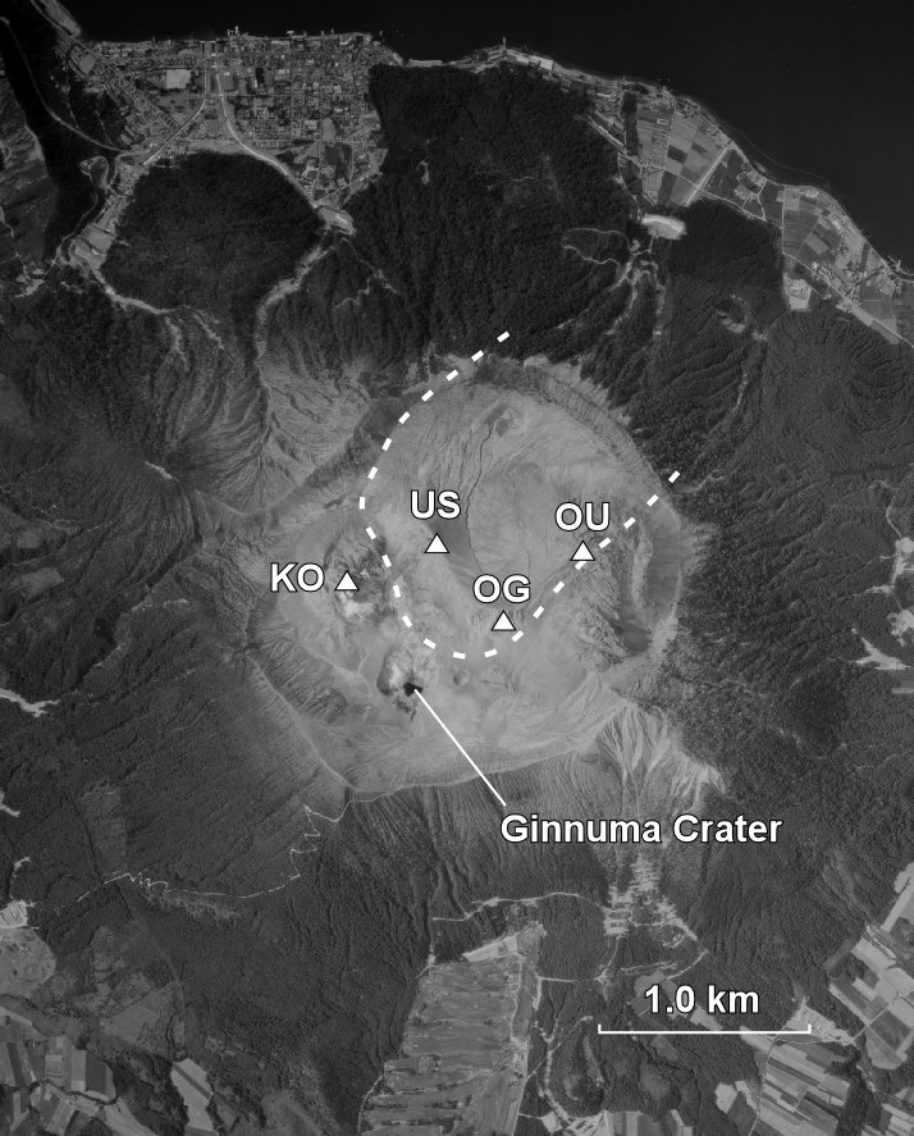
US
OU
KO
OG
Ginnuma Crater
1.0 km

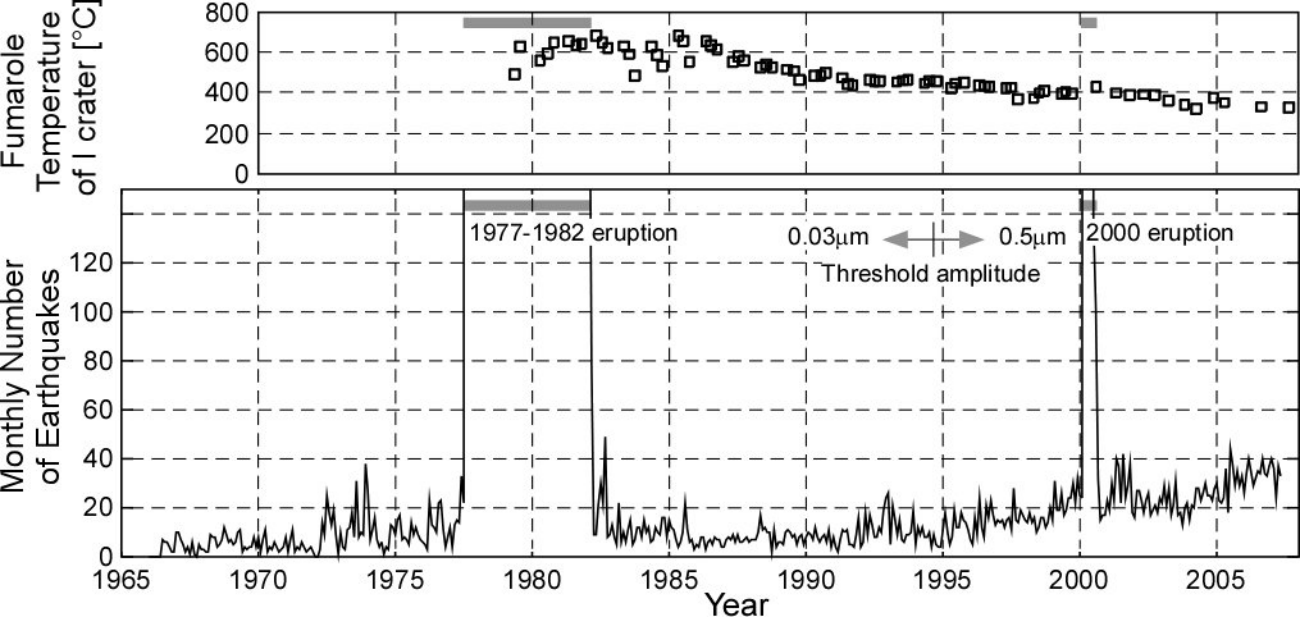
Fumarole Temperature of I crater [°C]
800
600
400
200
0
1977-1982 eruption
0.03μm
0.5μm
2000 eruption
Threshold amplitude
Monthly Number of Earthquakes
120
100
80
60
40
20
0
1965
1970
1975
1980
1985
1990
1995
2000
2005
Year

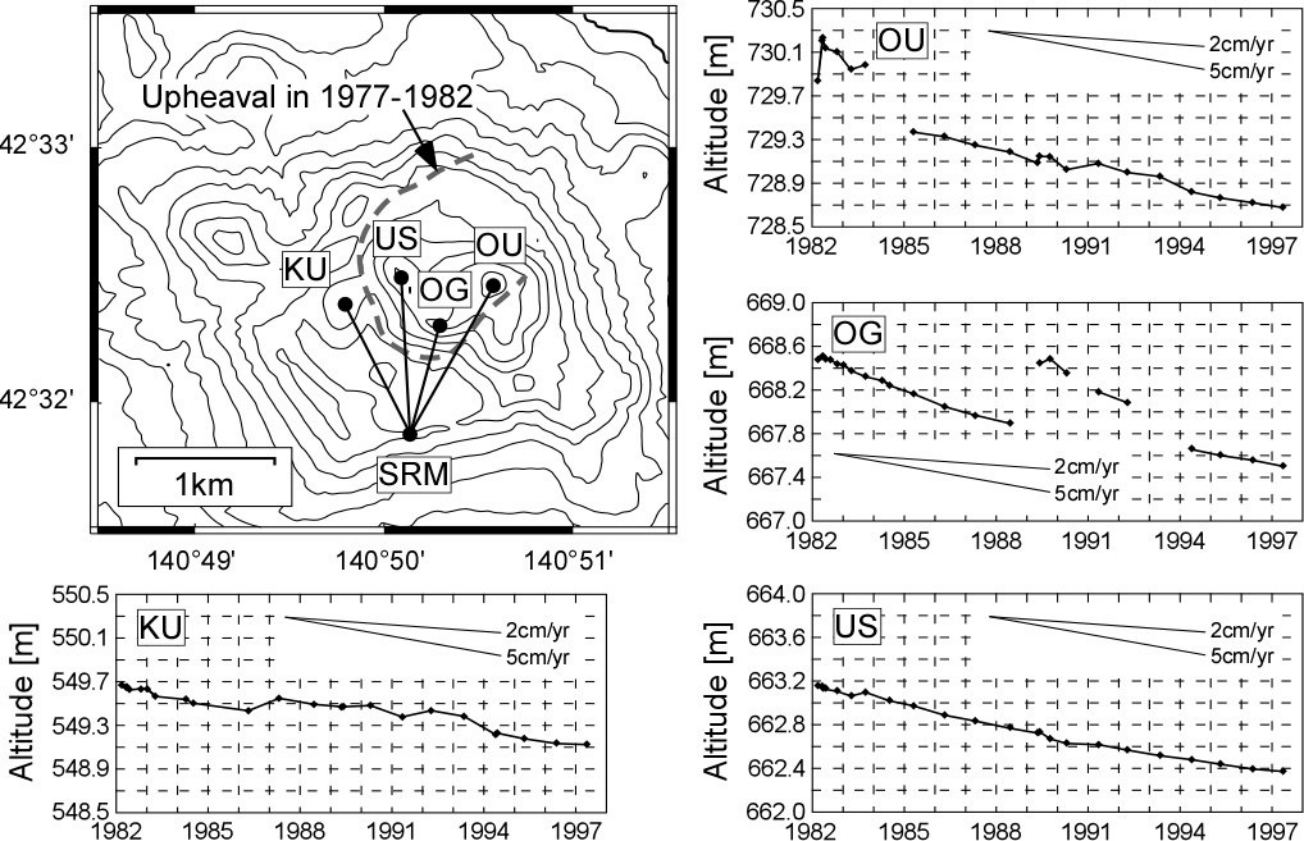
Upheaval in 1977-1982
42°33'
42°32'
KU
US
OU
OG
SRM
1km
140°49'
140°50'
140°51'
OU
OG
KU
US
Altitude [m]
2cm/yr
5cm/yr
730.5
730.1
729.7
729.3
728.9
728.5
669.0
668.6
668.2
667.8
667.4
667.0
550.5
550.1
549.7
549.3
548.9
548.5
664.0
663.6
663.2
662.8
662.4
662.0
1982
1985
1988
1991
1994
1997

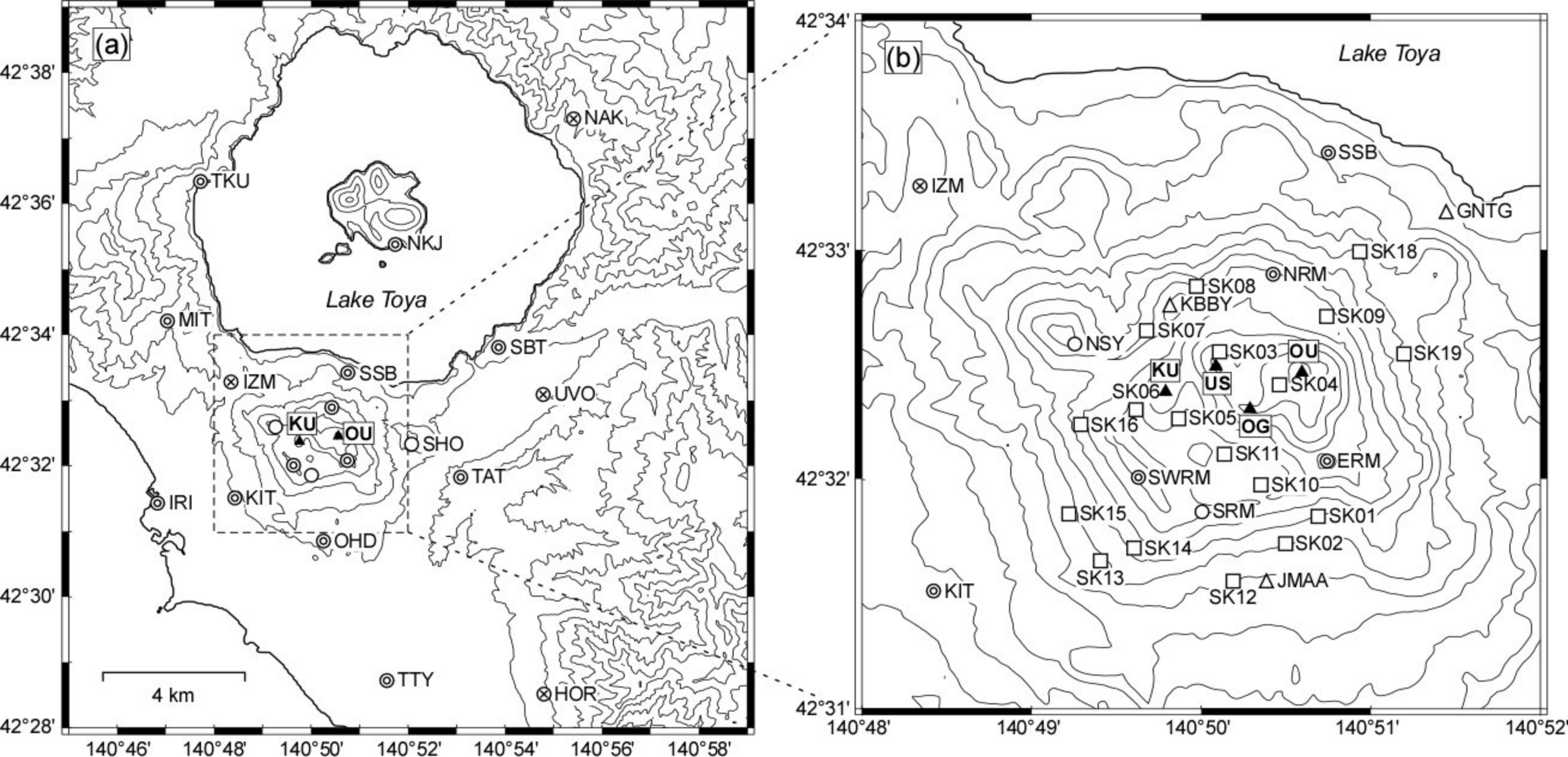
(a)
42°38'
42°36'
42°34'
42°32'
42°30'
42°28'
140°46'
140°48'
140°50'
140°52'
140°54'
140°56'
140°58'
NAK
TKU
NKJ
Lake Toya
MIT
SBT
IZM
SSB
UVO
KU
OU
SHO
TAT
IRI
KIT
OHD
TTY
HOR
4 km
(b)
42°34'
42°33'
42°32'
42°31'
140°48'
140°49'
140°50'
140°51'
140°52'
Lake Toya
SSB
IZM
GNTG
SK18
NRM
SK08
KBBY
SK09
SK07
NSY
SK03
OU
SK19
KU
US
SK06
SK04
SK16
SK05
OG
SK11
ERM
SWRM
SK10
SK15
SRM
SK01
SK14
SK02
SK13
JMAA
SK12
KIT

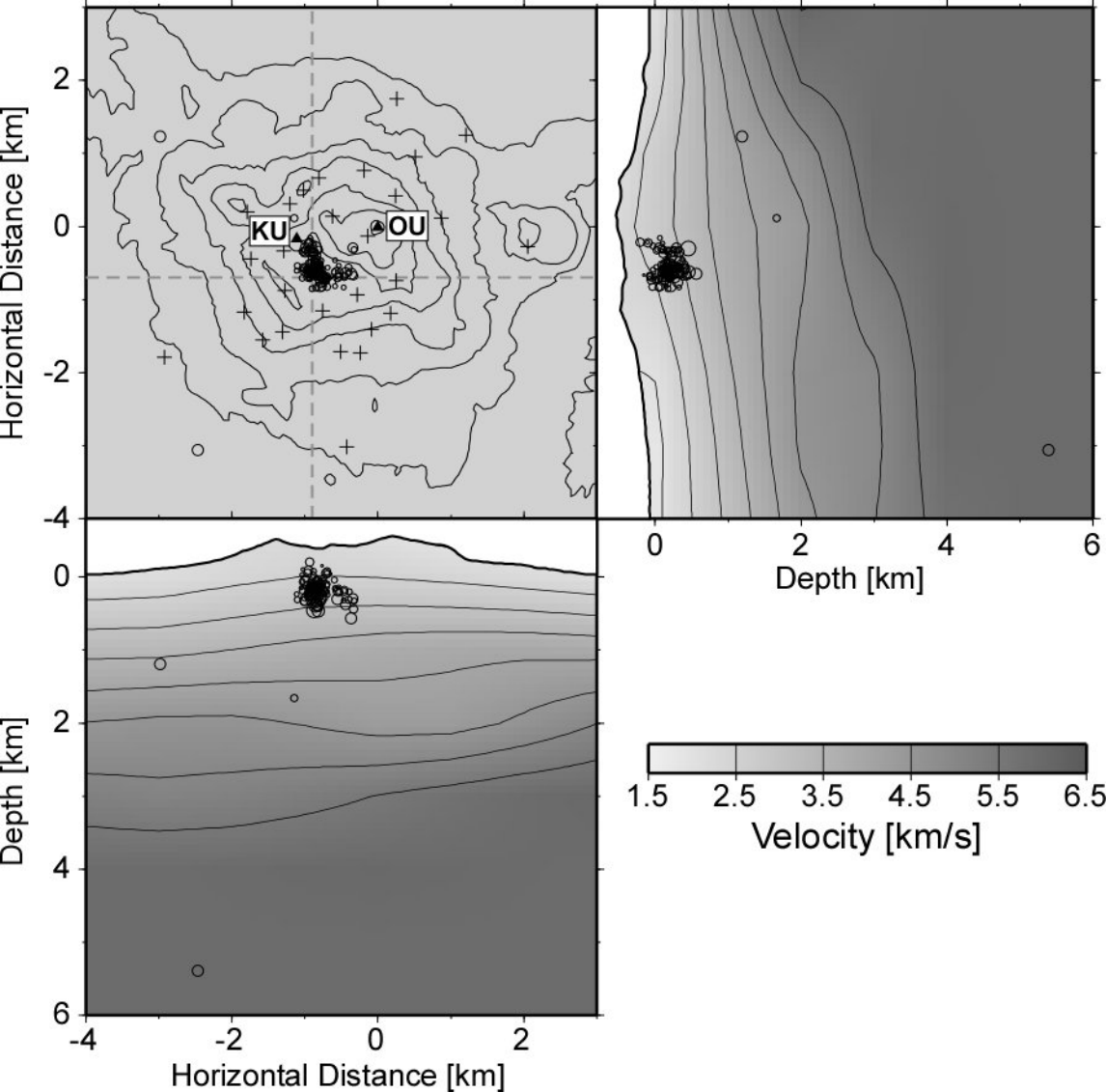
KU
OU
Horizontal Distance [km]
Depth [km]
Depth [km]
Horizontal Distance [km]
1.5 2.5 3.5 4.5 5.5 6.5
Velocity [km/s]

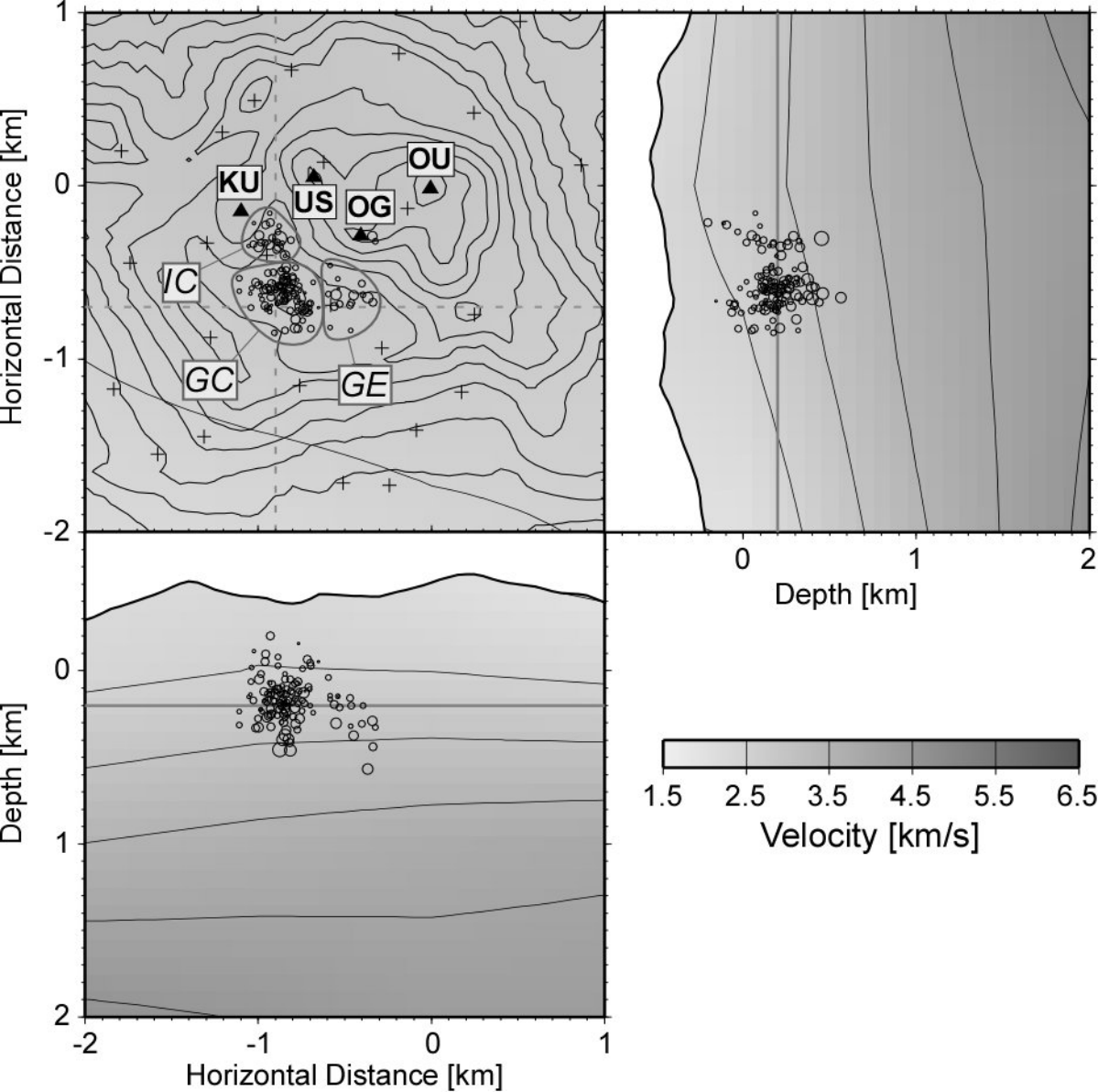
KU
US
OG
OU
IC
GC
GE
Horizontal Distance [km]
Depth [km]
Depth [km]
Horizontal Distance [km]
1.5
2.5
3.5
4.5
5.5
6.5
Velocity [km/s]

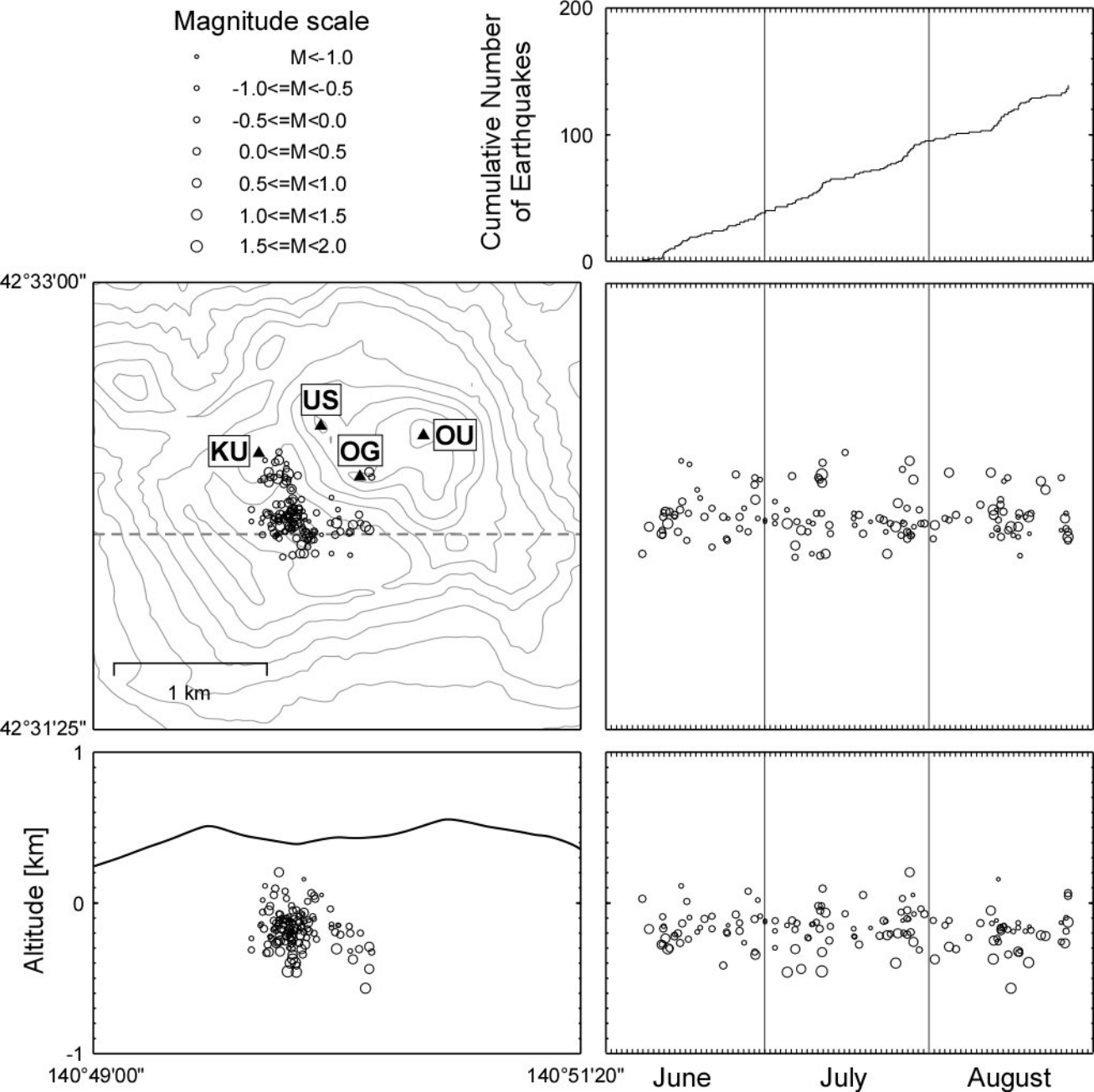
Magnitude scale
M<-1.0
-1.0<=M<-0.5
-0.5<=M<0.0
0.0<=M<0.5
0.5<=M<1.0
1.0<=M<1.5
1.5<=M<2.0
Cumulative Number of Earthquakes
200
100
0
42°33'00"
42°31'25"
US
KU
OG
OU
1 km
Altitude [km]
1
0
-1
140°49'00"
140°51'20"
June
July
August

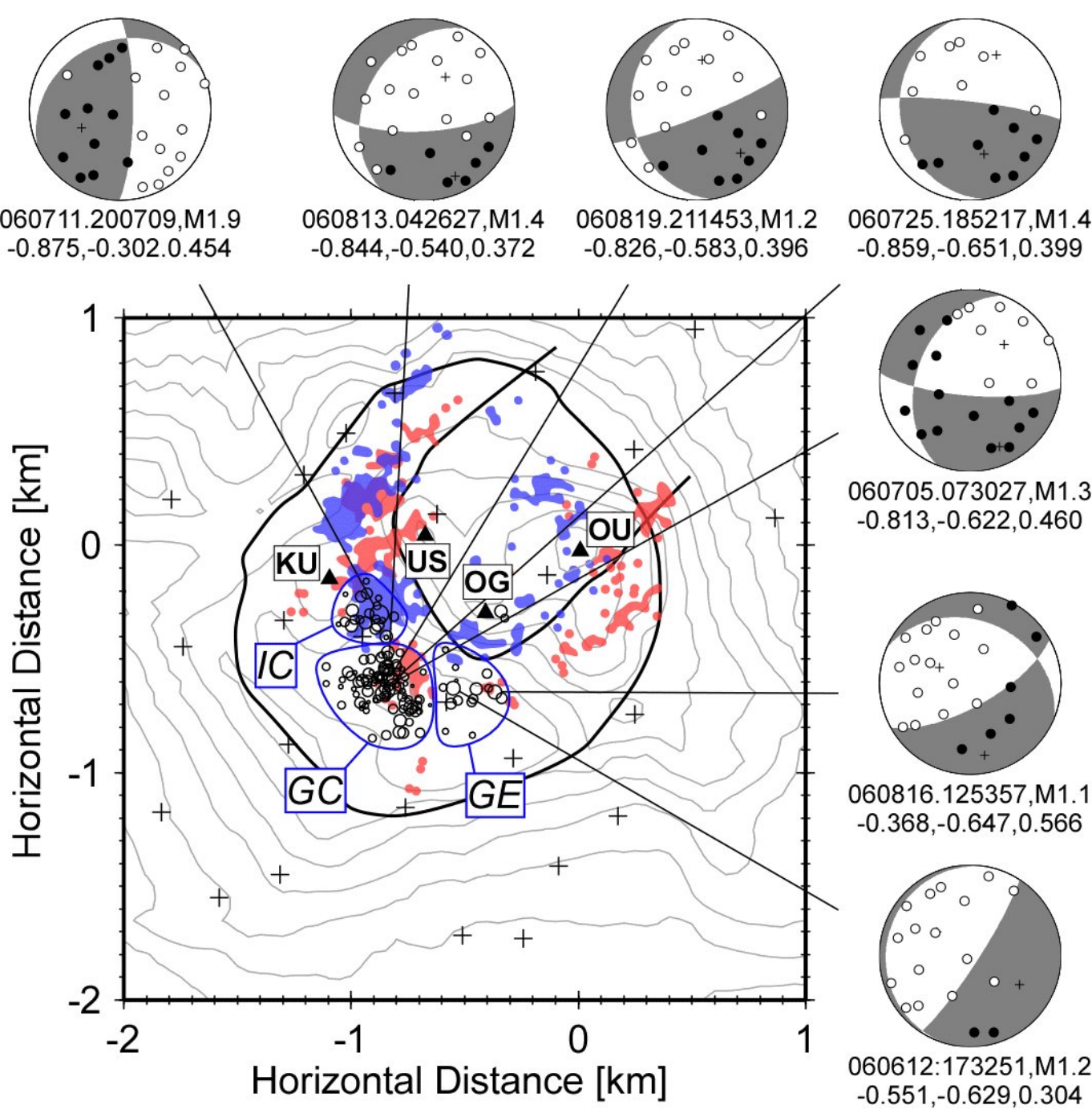
060711.200709,M1.9
-0.875,-0.302.0.454
060813.042627,M1.4
-0.844,-0.540,0.372
060819.211453,M1.2
-0.826,-0.583,0.396
060725.185217,M1.4
-0.859,-0.651,0.399
060705.073027,M1.3
-0.813,-0.622,0.460
060816.125357,M1.1
-0.368,-0.647,0.566
060612:173251,M1.2
-0.551,-0.629,0.304
KU
US
OG
OU
IC
GC
GE
Horizontal Distance [km]
Horizontal Distance [km]
1
0
-1
-2
-2
-1
0
1

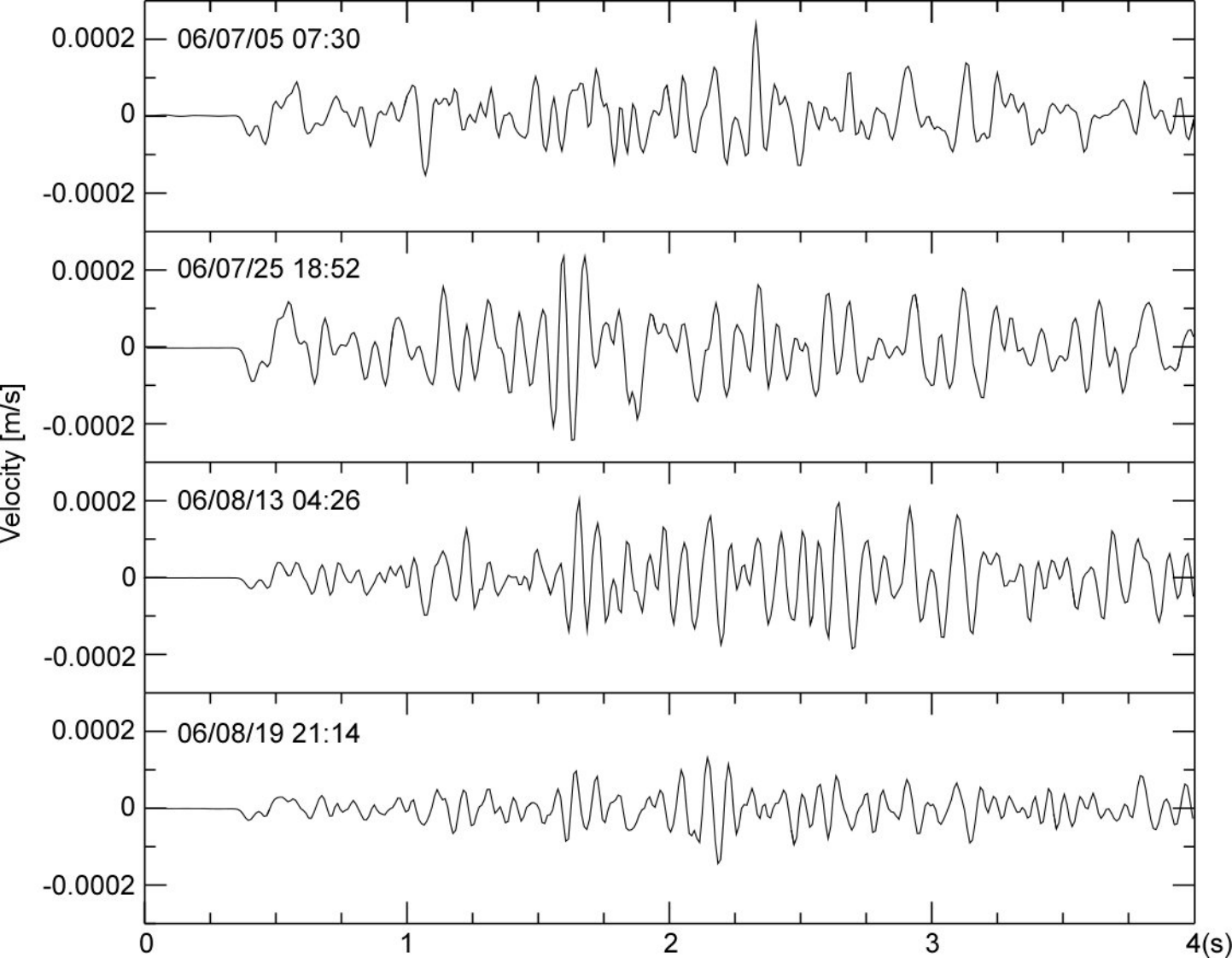
06/07/05 07:30
06/07/25 18:52
06/08/13 04:26
06/08/19 21:14
0.0002
0
-0.0002
Velocity [m/s]
0
1
2
3
4(s)

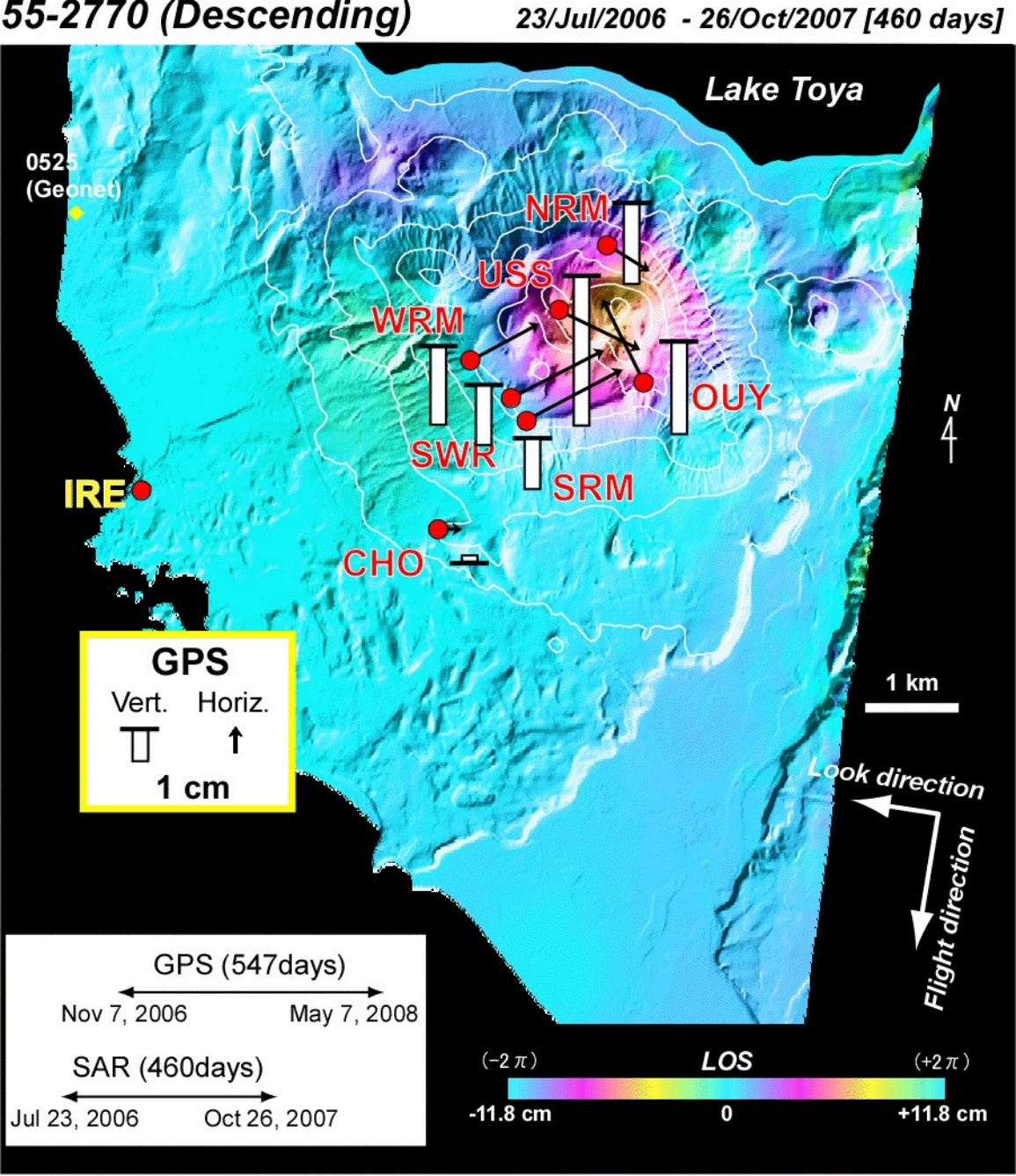
55-2770 (Descending)
23/Jul/2006 - 26/Oct/2007 [460 days]
Lake Toya
0525
(Geonet)
NRM
USS
WRM
OUY
SWR
SRM
IRE
CHO
N
GPS
Vert. Horiz.
1 cm
1 km
Look direction
Flight direction
GPS (547days)
Nov 7, 2006
May 7, 2008
SAR (460days)
Jul 23, 2006
Oct 26, 2007
(−2 π)
LOS
(+2 π)
-11.8 cm
0
+11.8 cm

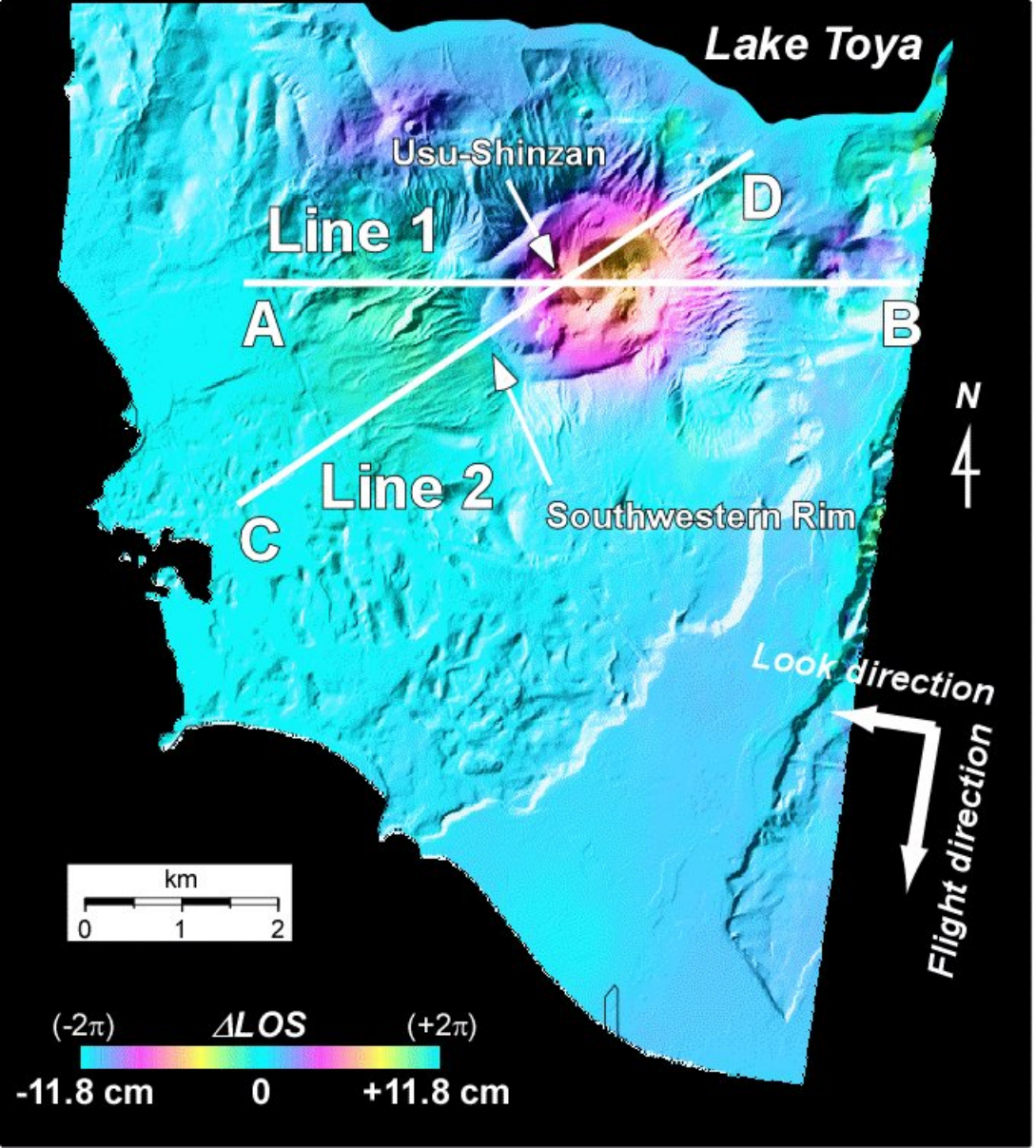
Lake Toya
Usu-Shinzan
Line 1
A
B
D
Line 2
C
Southwestern Rim
N
km
0
1
2
Look direction
Flight direction
(-2π)
ΔLOS
(+2π)
-11.8 cm
0
+11.8 cm

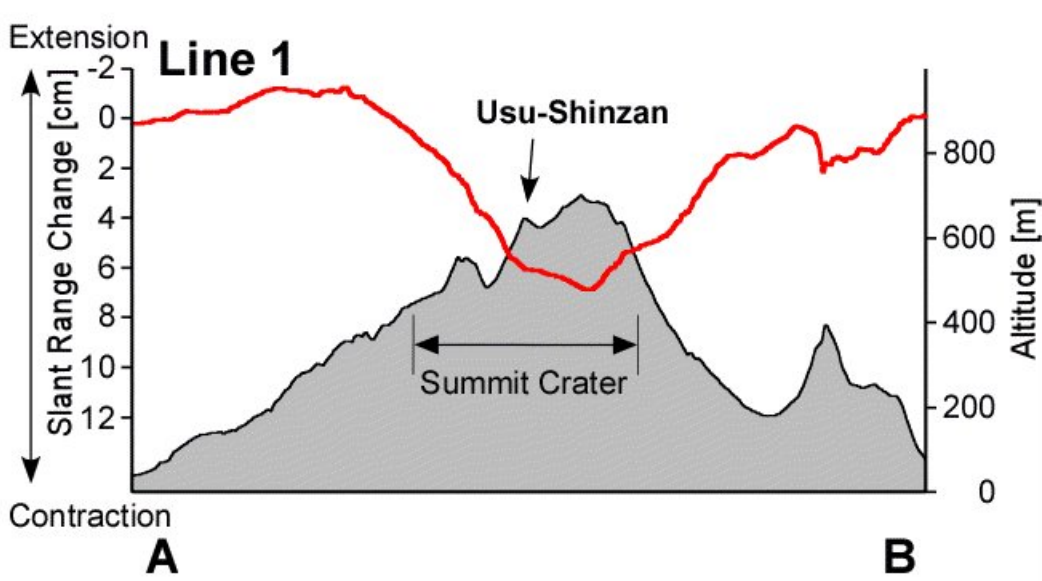
Extension
Line 1
Usu-Shinzan
Slant Range Change [cm]
-2
0
2
4
6
8
10
12
Summit Crater
800
600
400
200
0
Altitude [m]
Contraction
A
B

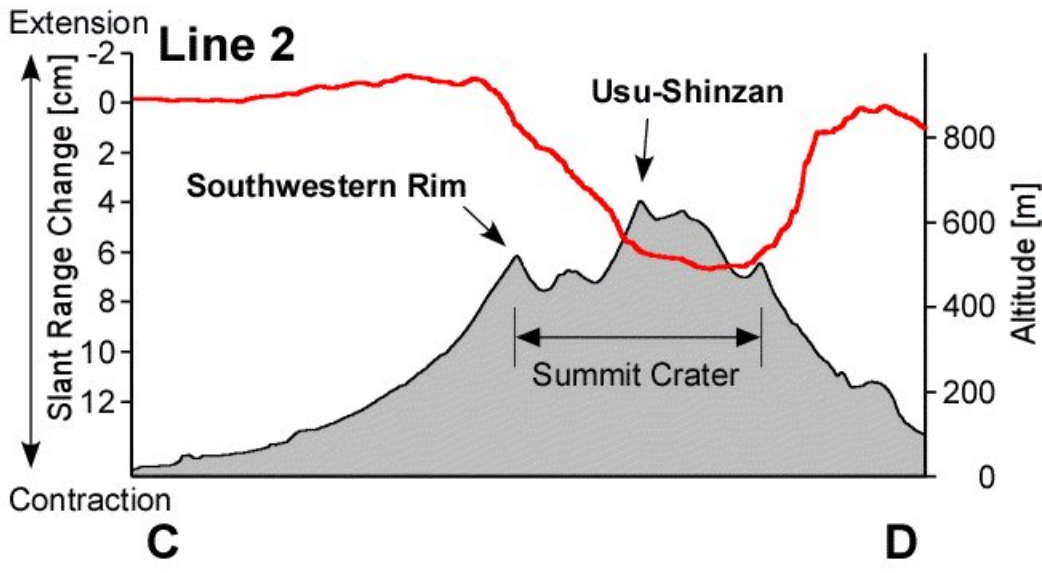
Extension
Line 2
Usu-Shinzan
Southwestern Rim
Slant Range Change [cm]
-2
0
2
4
6
8
10
12
Summit Crater
800
600
400
200
0
Altitude [m]
Contraction
C
D

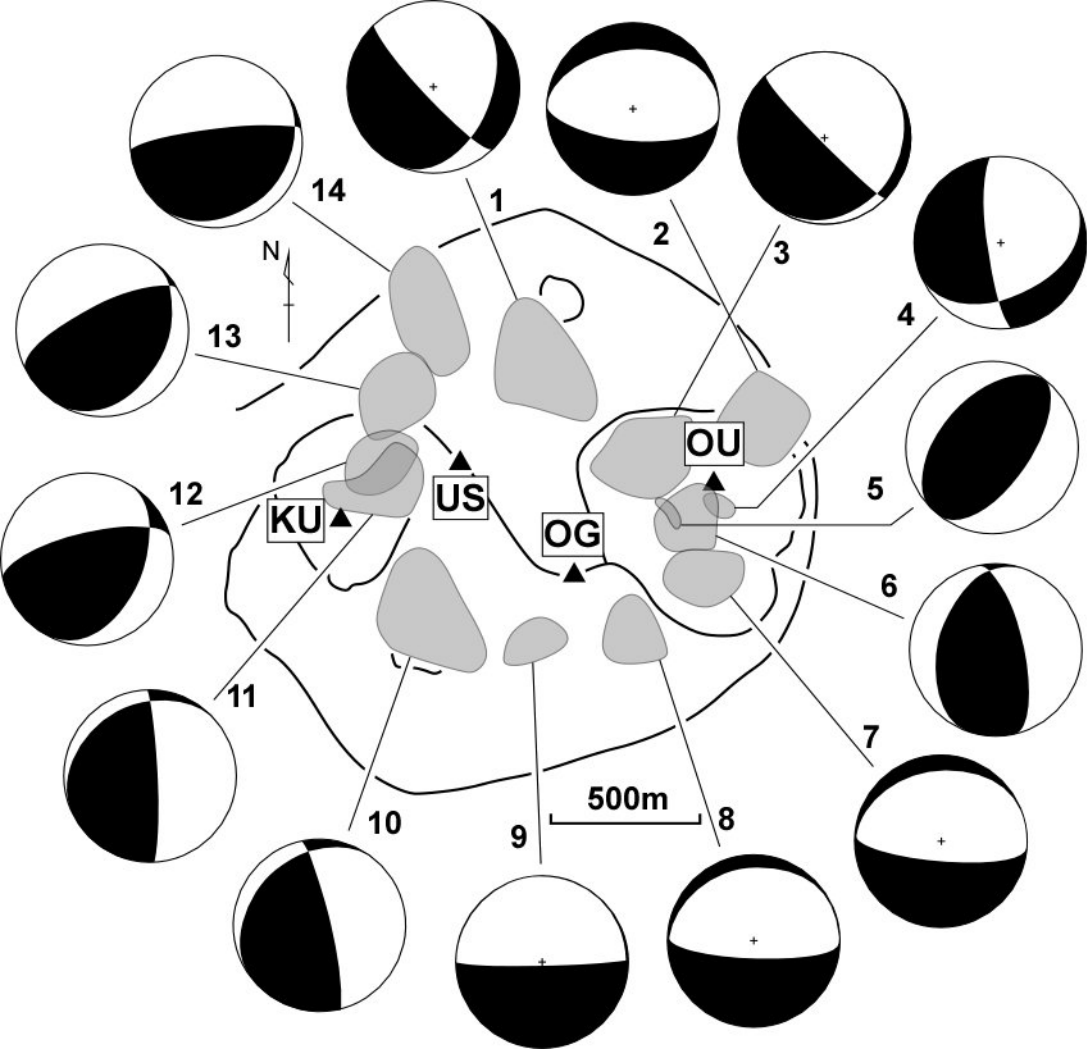
1
2
3
4
5
6
7
8
9
10
11
12
13
14
N
OU
US
OG
KU
500m

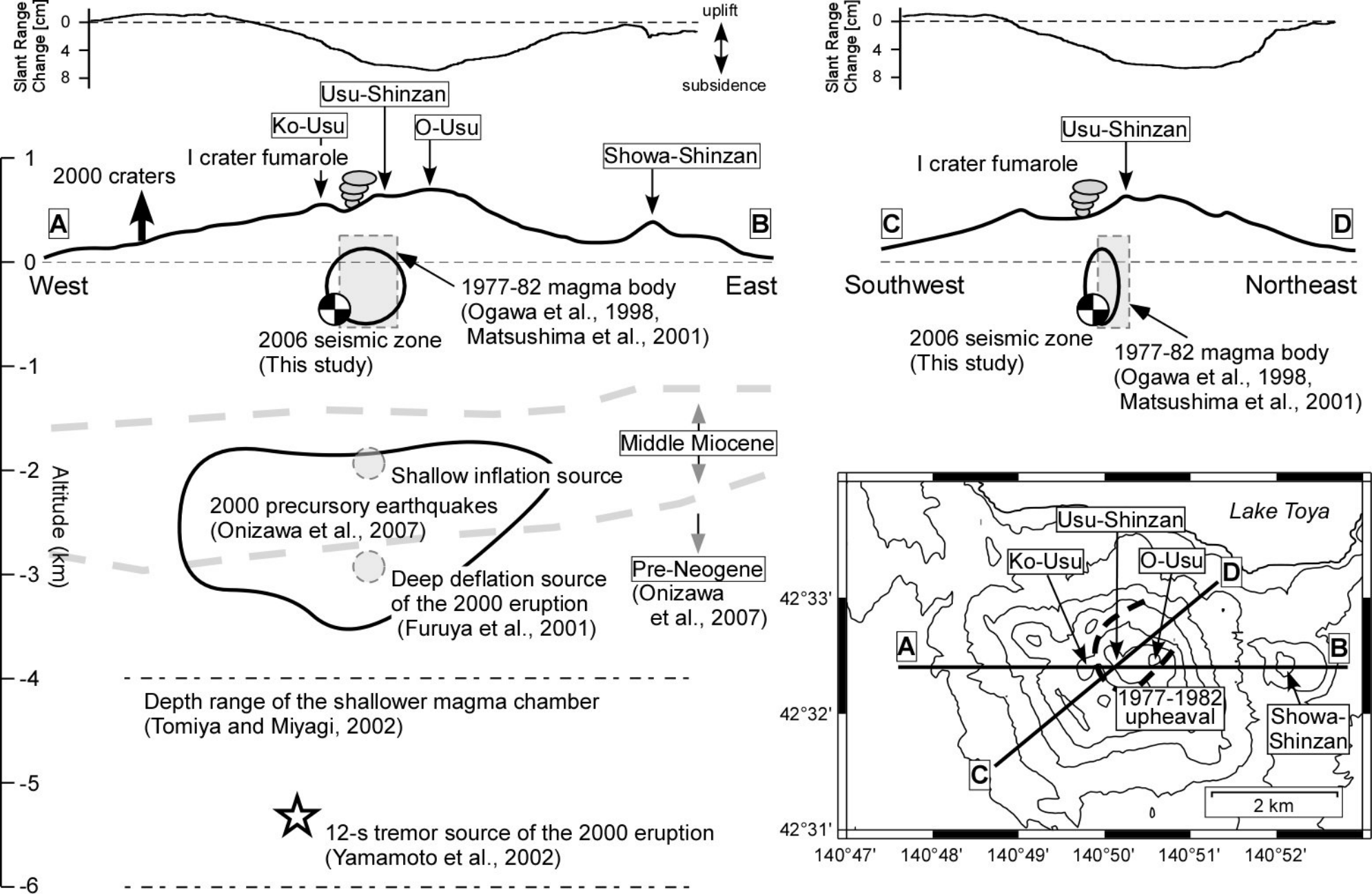
Slant Range Change [cm]
0
4
8
uplift
subsidence
Usu-Shinzan
Ko-Usu
O-Usu
I crater fumarole
2000 craters
Showa-Shinzan
A
B
West
East
1977-82 magma body
(Ogawa et al., 1998,
Matsushima et al., 2001)
2006 seismic zone
(This study)
Slant Range Change [cm]
0
4
8
Usu-Shinzan
I crater fumarole
C
D
Southwest
Northeast
2006 seismic zone
(This study)
1977-82 magma body
(Ogawa et al., 1998,
Matsushima et al., 2001)
1
0
-1
-2
-3
-4
-5
-6
Altitude (km)
Middle Miocene
Shallow inflation source
2000 precursory earthquakes
(Onizawa et al., 2007)
Deep deflation source
of the 2000 eruption
(Furuya et al., 2001)
Pre-Neogene
(Onizawa
et al., 2007)
Depth range of the shallower magma chamber
(Tomiya and Miyagi, 2002)
12-s tremor source of the 2000 eruption
(Yamamoto et al., 2002)
Lake Toya
Usu-Shinzan
Ko-Usu
O-Usu
D
A
B
C
1977-1982
upheaval
Showa-
Shinzan
2 km
42°33'
42°32'
42°31'
140°47'
140°48'
140°49'
140°50'
140°51'
140°52'